Subduction interface processes recorded by eclogite-facies shear zones (Monviso, W. Alps)

Samuel Angiboust, Philippe Agard, Hugues Raimbourg, Philippe Yamato, Benjamin Huet

Subduction interface processes

recorded by eclogite-facies shear zones (Monviso, W. Alps)

Angiboust, S., Agard, P.

ISTEP, Université Paris 06-UPMC, UMR CNRS 7193, 75252 Cedex 05 PARIS, France

Raimbourg, H.

ISTO, UMR CNRS 6113, Campus Géosciences, 1A rue de la Férolerie, 45071 ORLEANS cedex 2, France

Yamato, P.

Geosciences Rennes, UMR CNRS 6118, Université de Rennes1 Campus Beaulieu CS 74205, F-35 042 Rennes Cedex France

Huet, B.

Department for Geodynamics and Sedimentology, University of Vienna, Althanstrasse 14, A-1090 Vienna, Austria

***Corresponding author**: Samuel ANGIBOUST*

ISTeP, Université Pierre et Marie Curie, Case 129, 46-00 3^{e}, 4, place Jussieu, 75252 PARIS Cedex 05, France

00 33 1 44274904 (Tel) / 00 33 1 44275085 (Fax)

samuel.angiboust@upmc.fr

Abstract

The Monviso ophiolite Lago Superiore Unit constitutes a well-preserved, almost continuous upper fragment of oceanic lithosphere subducted at c. 80 km depth, thereby providing a unique opportunity to study mechanical coupling processes and meter-scale fluid-rock interactions occurring at such depths in present-day subduction zones. It is made of (i) a variably thick (50-500m) section of eclogitized basaltic crust (associated with minor calcschist lenses) overlying a 100-400m thick metagabbroic body and of (ii) a c. 1km thick serpentinite sole. We herein focus on the three major eclogite-facies shear zones found at the top of the unit, at the boundary between basalts and gabbros, and between gabbros and serpentinites, respectively. Strain localization occurred at lithological interfaces, irrespective of material strength. While ductile deformation dominates along the shear zones, local brittle behaviour is demonstrated by the existence of numerous eclogite breccias of Fe-Ti metagabbros and widespread garnet fractures, possibly linked with intermediate-depth eclogite-facies (micro)seismicity. These m- to hm-sized fragments of Fe-Ti metagabbros were later sheared and disseminated within serpentinite schists along the gabbro-serpentinite boundary (Lower Shear zone; LSZ). Pervasive and focused fluid flow is attested in the LSZ by significant alteration of bulk rock compositions, weakening of the rocks and widespread crystallization of hydrous parageneses. By contrast, the Intermediate Shear zone (ISZ) shows evidence for more restricted, short-range fluid flow. The activity of both the ISZ and LSZ ceased during early lawsonite eclogite-facies exhumation, when deformation localized deeper within the serpentinite sole, allowing for the detachment (and preservation) of this large ophiolitic fragment.

***Keywords**: Subduction channel, shear zone, eclogite, fluids, Monviso ophiolite*

1. Introduction

Characterisation of subduction interface dynamics is crucial to understand lithospheric-scale coupling between plates, vertical movements, material recycling and to better assess seismic hazard. The subduction interface is the target of numerous geophysical (e.g., Zhao et al., 2002; Oncken et al., 2003; Ranero et al., 2003; Abers et al., 2006; Raimbourg et al., 2007; Hilairet et al., 2007) and numerical modelling investigations (e.g., Gerya et al., 2002; Yamato et al., 2007). A wealth of field observations constrain mechanical processes occurring along the seismogenic zone at depth where megathrust earthquakes occur (15-35km; Toyoshima, 1990; Ikesawa, 2003; Rowe et al., 2005; Bachmann et al., 2009; Meneghini et al., 2010; Fig. 1). In comparison, mechanical processes taking place deeper (>30-40 km) along the subduction interface, such as episodic tremor and slip events (Rogers and Dragert, 2003) or intermediate depth seismicity, are still poorly known due to the scarcity of well-preserved fault planes and shear zones within exhumed fragments detached beyond such depths (e.g. Austrheim and Andersen, 2004; John and Schenk, 2006; Healy et al., 2009; Fig. 1).

Large-scale, fossil shear zones from exhumed portions of subducted lithosphere may preserve the record of subduction interface processes (such as dynamic recrystallization, fluid flow and mass transfer) and shed light on interplate mechanical coupling and past seismic activity (e.g., White et al., 1980; Kirby, 1985; Handy et al., 1999; Montési and Hirth, 2003; John et al., 2009; Platt and Behr, 2011). However, contrary to eclogite facies shear zones from deeply subducted continental crust studied in the Norwegian Caledonides (e.g., Boundy et al., 1992; Fountain et al., 1994; Terry and Heidelbach, 2006; Raimbourg et al., 2007), few examples exist on large-scale, deeply subducted oceanic lithosphere remnants liable to give information on mechanisms acting during long-lived oceanic subduction (e.g., Philippot and Van Roermund, 1992; Hermann et al., 2000).

This paper aims at filling this gap and focuses on eclogite-facies shear zones formed at c. 80 km depth during oceanic subduction, which are found in the Monviso ophiolite, a well-preserved fragment of Tethyan oceanic lithosphere (W. Alps, Italy; Lombardo et al., 1978; Lagabrielle and Lemoine, 1997; Groppo and Castelli, 2010; Spandler et al., 2011; Angiboust et al., 2011).

We herein present detailed petrological and deformation data, from the kilometer scale to the mineral scale, on the three largest shear zones found in the Monviso ophiolite, as identified from previous mapping and recently published P-T determinations (Angiboust et al., 2011). The field relationships and petrography, mineralogy and chemistry of the three major shear zones are successively presented and a detailed petro-tectonic evolution is then proposed. We then discuss implications for fluid-flow, strain partitioning and subduction dynamics, and for the detachment and migration of km-scale fragments along the subduction interface.

2. Geological setting and structure of the Lago Superiore Unit

The Western Alps result from successive subduction, accretion and collision between the European and Apulian/African plates from the Cretaceous to the Oligocene (Coward et al., 1989; Polino et al., 1990; Agard et al., 2002; Rosenbaum and Lister, 2005). The internal Western Alps represent the W-verging stack of continental and oceanic nappes formed during subduction and (partial) exhumation of the Jurassic Tethyan seafloor and associated European thinned margin below the Apulian plate (e.g., Bearth, 1967; Dal Piaz et al., 1972; Agard et al., 2002; Rubatto and Hermann, 2003; Oberhänsli and Goffé, 2004; Angiboust et al., 2009; Beltrando et al., 2010). Remnants of this slow-spreading ocean form the Liguro-Piemontese domain, now sandwiched between the Penninic front and eclogitized portions of the European continental margin (e.g., Dora Maira, Gran Paradiso; Fig. 2, inset). Eclogitized portions of the Liguro-Piemontese oceanic lithosphere are found 200 km along-strike, from the Zermatt-Saas area (in the north) to the

Monviso area (in the south), and constitute some of the largest and deepest ophiolitic slices detached from a subduction zone (Reinecke, 1998; Bucher et al., 2005; Angiboust et al., 2009).

The southern extent of the Liguro-Piemontese domain can be divided in two main tectono-metamorphic domains. To the west (Queyras area), the external Liguro-Piemontese zone corresponds to a fossil accretionary wedge, the Schistes Lustrés domain *s.s.*, where m- to hm-sized blocks and lenses of mafics and ultramafics are embedded in blueschist-facies, late Mesozoic metasedimentary rocks (e.g., Lagabrielle et al., 1984; Deville et al., 1992; Schwartz et al., 2000; Agard et al., 2001, 2002; Tricart et al., 2004; Fig. 2, inset). To the East, the Monviso ophiolite forms the structural base of the Liguro-Piemontese domain and is separated from the adjacent Schistes Lustrés *s.s.* domain by an extensional shear zone (Ballèvre et al., 1990). The Monviso ophiolite is in turn separated from the underlying continental Dora Maira massif (Sampeyre and Dronero units) by another extensional shear zone (Blake and Jayko, 1990; Fig. 2a,b). These deep tectonic contacts, originally thrust planes, were thus reactivated as detachment zones during the Monviso exhumation history (e.g. Philippot and Van Roermund, 1992).

Based on tectono-stratigraphy, the Monviso ophiolitic massif was earlier divided into six units separated by W-dipping ductile tectonic contacts (Lombardo et al., 1978; Schwartz et al., 2001). All the rocks of the massif show evidence for recrystallization under eclogite-facies conditions followed by retrogression under epidote-blueschist facies and greenschist facies (Lombardo et al., 1978; Blake et al., 1995). Ages for eclogitization of the ophiolite range between 50 and 40 Ma (Monié and Philippot, 1989; Duchêne et al., 1997; Cliff et al., 1998; Rubatto and Hermann, 2003). Several studies suggested variable maximum P-T conditions for the Monviso ophiolite (from *c.* 450°C/12 kbar to 620°C/24 kbar; Blake et al., 1995; Messiga et al., 1999; Schwartz et al., 2001) and argued for the presence of a deep subduction mélange where tectonic slices detached from different depths accumulated in a weak serpentinized subduction channel (e.g., Guillot et al., 2004). However, Angiboust et al. (2011) recently demonstrated that the Monviso ophiolite can be divided in two main coherent tectono-metamorphic units (Fig. 2b): (i)

the Monviso Unit to the W, which reached *c.* 480°C/ 22 kbar and (ii) the Lago Superiore Unit to the E, which recrystallized within lawsonite eclogite facies close to the coesite stability field (*c.* 550°C/ 26 kbar; similar estimates were obtained on a lawsonite-eclogite assemblage by Groppo and Castelli, 2010). These two units are separated by a ductile shear zone named "Upper Shear Zone" (USZ) in this study (Fig. 2).

The Lago Superiore Unit is a well-preserved, relatively undisturbed section of oceanic lithosphere, cut across by two major shear zones (referred to as the "Intermediate" and "Lower Shear Zones": ISZ and LSZ; Fig.2b; Philippot and Kienast, 1989; Angiboust et al., 2011). The upper portion of the section is composed of a variably thick and heterogeneous, dominantly mafic sequence containing (i) metabasalts and associated interpillow material (60-80%), (ii) metadiabases and Fe-Ti metagabbro layers (10-20%) and (iii) calcschists (5-10%; Fig.2b). The middle part of the section is composed of a 200-300m thick Mg-Al metagabbro capped by a discontinuous (generally 5-20m thick) layer of Fe-Ti metagabbros. The bottom of the sequence is mainly composed of serpentinites derived from hydrothermally altered abyssal peridotites (Monviso, 1980; Hattori and Guillot, 2007; Figs.2b, 3a).

3. Field observations in the three major shear zones

The three main shear zones, which cut across the Monviso ophiolite, are either localized at the boundary between units with different P-T histories (USZ) or along major lithological boundaries (ISZ, LSZ; Figs. 2b, 3). By contrast, m-sized shear zones found in the field show limited spatial continuity and lack well-developed mylonites or blocks embedded in serpentinite. For the sake of clarity, field observations for each of the shear zones are summarized in Table 1 and detailed geological maps of the shear zones are given as Supplementary material 1.

3.1 The Upper Shear Zone (USZ)

The USZ can be followed over 15 kilometers from Colle Armoine in the north to south of Passo Gallarino in the south (Fig. 2a). This USZ is lined up by a variably thick (between 1 and 30m) serpentinite sliver, in which m-sized flattened lenses of Fe-Ti metagabbros are randomly dispersed, together with rare Mg-Al gabbro lenses and metasediments (dominantly calcschists). Metabasaltic rocks forming the lower margin of the USZ are commonly dragged and sliced along the shear zone. Meter-sized mylonite serpentinite slivers are also interleaved with strongly retrogressed metabasalts in the vicinity of the USZ. Importantly, eclogitic lenses found along the USZ do not record evidence for strong and pervasive eclogite-facies mylonitization as for other shear zones deeper in the ophiolite pile (see below). The USZ was intensively reactivated as an extensional detachment zone during later exhumation stages, as testified by the formation of ubiquitous W-dipping shear bands and L-tectonites at the transition between epidote blueschist facies and greenschist facies conditions (9kbar, 420°C; Schwartz et al., 2000).

3.2 *The Intermediate Shear Zone (ISZ)*

The ISZ, which is more limited spatially than the other two, is well expressed in the Lago Superiore area and pinches out southwards in the Viso Mozzo area and northwards (Fig. 2a, Fig. 3a). In the Lago Superiore area (Supplementary material 1a), Mg-Al metagabbros, which constitute the bulk of the sequence, are capped by a 2-50 meter-thick discontinuous sequence of dark Fe-Ti metagabbros (ISZ-17; Fig. 3a) exhibiting a mylonitic foliation sub-parallel to the ISZ. The absence of large porphyroblasts in the mylonitic foliation, however, prevents identification of the dominant sense of shear.

These eclogites are heterogeneously deformed, showing an alternation of highly and intermediately strained samples at the outcrop scale (Philippot and Kienast, 1989). Intermediate to highly strained mylonites represent over 90 % of the volume outcrop in the Lago Superiore area.

High strain, non-coaxial deformation and folding interferences led to the formation of N-S trending cigar-shaped boudins (10m x 1m) in the Lago Superiore area (Philippot, 1987). Tensile fractures with fibrous omphacite perpendicular to the vein walls (and with the mylonitic foliation only occasionally deflected around these veins) represent a few percents of the rock volume (Philippot and Kienast, 1989). The different generations of omphacite epitaxial fillings along these veins were interpreted as marking successive incremental crack-seal processes associated with mylonitization and cm-scale, fluid-assisted mass transfer (Nadeau et al., 1993).

Several metabasaltic lenses, and to a minor extent metasediments, are found along the ISZ within serpentinite mylonites, lying subparallel to the main gently dipping foliation (~N005 15-30° W). P-T estimates show that these rocks underwent a metamorphic history similar to that of the walls of the shear zone (Angiboust et al., 2011). The apparent meter-scale structural complexity therefore results from a tectonic juxtaposition of rocks constituting the walls of the ISZ together with variably thick serpentinite slivers (0-10m; Table 1). The presence of an allochtonous serpentinite sliver between gabbros and basalts (Fig. 2a, Lago Superiore Area) indicates that the ophiolitic sequence was disrupted along the ISZ. Retrogression under epidote blueschist-facies is attested by the formation of glaucophane, chlorite, epidote and albite instead of garnet and omphacite). It dominantly affects the metabasalts from the hanging wall, whereas mylonitized Fe-Ti metagabbros are remarkably well-preserved.

3.3 *The Lower Shear Zone (LSZ)*

The LSZ runs at the base of the main Mg-Al gabbro body, at the boundary with the underlying serpentinite sole, and can be traced over 15 km in the studied area from Rocce Fons in the north to Colle di Luca in the south (Fig. 2a). The LSZ ranges in thickness from 40 to 150 m (Supplementary material 1b, c, d). The upper boundary of the LSZ is well defined by the Mg-Al gabbro interface but its lower margin, towards the serpentinite sole, is much more diffuse.

Finite deformation linked to the activity of the LSZ is characterized by (i) a W-dipping foliation (generally 20-30°) and the flattening of the Mg-Al gabbros of the hanging wall and (ii) an extremely pervasive schistosity in serpentinites. This serpentinized tectonic contact is lined by many irregularly dispersed lenses and aggregates of metagabbroic and metasedimentary rocks (Fig. 2b; Table 1). Rare lenses of metasediments (mainly calcschists, carbonates and garnet-chloritoid quartzites) are intercalated within serpentinites and metagabbro aggregates in the LSZ. Most of these flattened lenses are generally meter-sized except a large lens located at the southeast of the Lago Superiore reaching several hundred meters in length and ca. 50m in thickness (Supplementary Material 1d, Fig.2a; Fig. 3a) showing slightly higher maximum temperatures than adjacent rocks (Tmax=550-570°C vs. 530-550°C, respectively; see Angiboust et al., 2011). Rare meter-sized blocks of jadeitite (Compagnoni et al., 2007) after plagiogranite and rodingite veins (Lombardo et al., 1978; Castelli et al., 2002) are found in blocks and veins in the LSZ and within the underlying serpentinite sole, respectively. Metabasalts were neither observed within the LSZ nor within the serpentinite sole.

Fe-Ti metagabbros generally constitute large (10-20m-sized) rounded aggregates, internally made of several independent, rounded blocks (Fig. 3b-d), wrapped by a mixture of antigorite schists, tremolite schists and talcschists. The abundance of these small rounded fragments (0.1-0.5m sized), dispersed within the serpentinite in the vicinity of the major aggregates decrease away from the aggregate core. Importantly, small (<20cm) angular mylonite fragments are dispersed upon the rough block surface (Fig. 3b) and cemented by an omphacite-rich matrix.

Some of the meter-scale blocks are made of eclogitic breccias (Fig.3e,f), where internal rotation is attested by the strong variability in strike and dip of the main mylonitic foliation planes (Fig. 3f) and omphacite cementation is also conspicuous.

Fe-Ti eclogitic blocks expose remarkably well-preserved peak mylonitic assemblages and underwent only minor and very localized retrogression under epidote blueschist-facies and

greenschist facies (Table 1). These rocks are characterized by the ubiquitous presence of whitish layers or patchy aggregates (up to 1cm in length) of pseudomorphs after lawsonite, which is now dominantly replaced by epidote and paragonite (e.g. Lombardo et al., 1978; Fig. 4). They occur either along the mylonitic foliation (Fig.4a,d) but also as porphyroblasts associated with omphacite or as vein-filling material (Fig.4a,b,c; Table 1). In locality LSZ-21 (Fig. 2a), a block exhibiting a mylonitic fabric is wrapped by a banded eclogite mainly composed of strongly folded, milky (0.5 to 2 cm-thick) layers of pseudomorphed lawsonite and foliated fined-grained omphacite (Fig. 4d). Primary crack-seal omphacite-bearing fractures similar to those from the ISZ near Lago Superiore, are locally preserved and commonly associated with pseudomorphed lawsonite veins (Fig.4a,c). Textural relationships with the mylonitic fabric are often erased by later ductile deformation.

4. Mineralogy of shear zones eclogites

Eighteen samples from the three main shear zones (Fig. 2a) were selected from a set of 75 samples collected across the study area. We focus below on the eclogitic Fe-Ti gabbro with well-preserved peak assemblages and the extent to which they record the activity of these shear zones beyond 50 km depth. The detailed peak rock paragenesis are presented in Table 2. Analytical methods used to track mineralogical and compositional changes are described in Appendix A.

4.1 Upper Shear Zone eclogites (USZ)

Rare lenses of eclogitized Fe-Ti gabbros, locally retrogressed under blueschist-facies conditions, are dispersed throughout the USZ serpentinites. One characteristic sample was collected at the south of rifugio Sella (USZ-69; Fig. 2a, 5a). The texture of these low strain Fe-Ti

metagabbros consists of former corona features with garnet growing at the boundary of pseudomorphed magmatic crystals (see also Lombardo et al., 1978, Pognante and Kienast, 1987, Philippot and Von Roermund, 1992). Clinopyroxene porphyroblasts in sample USZ-69 have been rotated, fractured and disseminated along the foliation plane. Plastic deformation is suggested by the elongated shape of recrystallized omphacite crystals. Garnet porphyroblasts are only rarely fractured (but not healed) and always show a typical "alpine" zoning pattern (i.e. Mn-Ca rich cores and Fe-Mg enriched rims; Fig. 5b; Supplementary material 2). Phengite is randomly dispersed in the clinopyroxene matrix and dismembered rutile ribbons after magmatic ilmenite define a crude foliation together with clinopyroxene. Brecciated garnet and eclogite-facies mylonites such as those described hereafter for the other shear zones have not been observed along the USZ.

4.2 Intermediate Shear Zone eclogites (ISZ)

These eclogites are characterized by a marked grain size reduction of omphacite down to 5-10 µm and a relatively strong crystal preferred orientation within the foliation plane, interpreted as the result of plastic dynamic recrystallization by dislocation creep (Lardeaux et al., 1986; Philippot and Kienast, 1989; Philippot and Van Roermund, 1992). Brittle deformation is attested by the presence of fractured, 10 to 300µm large garnet porphyroblasts (Figs. 5d-f; initially part of coronitic structures: Pognante and Kienast, 1987). Omphacite-cored atoll garnet commonly occurs along the mylonitic foliation (Fig. 5c) but is systematically absent from low-strained Fe-Ti metagabbros. Phengite and glaucophane are rare (<0.5 vol. %) and generally aligned between omphacite crystals along the foliation. Pseudomorphs after lawsonite (much smaller than those from LSZ eclogites) generally occur as millimeter-sized ribbons or aggregates dispersed along the mylonitic foliation (sample ISZ-17, Fig. 5c).

Zoning patterns in garnet from ISZ mylonitic eclogites show embayments and healed fractures, suggesting a combination of dissolution and cementation (Fig. 5d). In the least fractured garnets, the original pattern with Ca/Mn-rich cores and Fe/Mg enriched rims is preserved. In addition, a sharp depletion in grossular content commonly occurs towards garnet rims, associated with a marked increase in pyrope content (Fig. 5e,f). The outermost parts of garnet rims are slightly enriched in Mn compared to garnet mantles (see Angiboust et al., 2011, for further chemical data on these garnets). Garnet filling the fractures, which are generally 5-10µm wide, is marked by a sharp enrichment in pyrope content too (from 8 mol. % to 16 mol. %; Supplementary material 3) and a slight depletion in grossularite and almandine contents. Some samples (ISZ-36a, ISZ-49) exhibit very small truncated garnet fragments with limited evidence of post-fracturing healing.

4.3 Lower Shear Zone eclogites (LSZ)

The LSZ contains numerous blocks of Fe-Ti metagabbros, some almost identical to those found in the ISZ. It nevertheless displays a much wider diversity of rock types than along the ISZ, suggesting a somewhat different post-mylonitic metamorphic history. A common feature to those diverse rock types only encountered in the LSZ is the presence of large and widespread hydrated mineral phases (Fig. 4b). By contrast, eclogites similar to those found in the ISZ will be referred here to as "dry" eclogites.

Within dry eclogites showing textural affinities with the highly strained ISZ eclogites (i.e., brecciation, cementation and grain-size reduction), some display a marked banding exemplified by almost monomineralic layers of garnet and omphacite (e.g., samples LSZ 52d and LSZ-21; Figs. 3d, 4d). Garnet-rich layers consist of over 75 vol. % of coalesced (50-100 µm-sized) garnet crystals with intergranular spaces filled by very fine grained omphacite (c. 10-30 µm).

Omphacite-rich layers contains less than 5% vol. garnet and preferentially host millimeter-sized aggregates of pseudomorphs after lawsonite (Fig. 3d).

Hydrated eclogites, which are found only in the LSZ (Figs 3b-f), can be grouped in two main categories:

- lawsonite-bearing eclogites (LSZ-17, 18, 21, 42 and 44)

Lawsonite-bearing eclogites occur on the rims of the blocks of Fe-Ti metagabbros, with centimetric (Figs. 4b,d) or millimetric lawsonite fringes along the mylonitic foliation (Fig. 4a). The rims of the smaller block fragments typically comprise garnet and omphacite-bearing layers with variable amounts (0-30 vol.%) of variably-sized euhedral lawsonite pseudomorphs (from 10µm to up to 1cm in length; Fig. 4b). Fragments scattered at the block surface are cemented by an omphacite-lawsonite+/-garnet assemblage that ranges from weakly (Fig. 4a,b) to highly strained (Fig. 4c). Garnet diameter ranges from 20µm up to 1cm (Fig. 4b). A complex fracture network is generally preserved within garnet, as in ISZ eclogites. These garnet crystals exhibit 10 to 20 µm-wide chemical oscillations associated with dissolution-precipitation processes (showing striking similarities to "cloudy" garnets described in Martin et al., 2011). One sample (LSZ-42; Fig. 5h) shows large phengite laths (0.5-4mm in length; Si^{4+} = [3.6-3.7 p.f.u]) in apparent textural equilibrium with subidioblastic garnet and fine grained omphacite aligned along the mylonitic foliation. Phengite has not been observed included within garnet cores. Small lawsonite pseudomorphs (c. 100µm long) are preferentially scattered in the phengite-rich layers (Fig. 5h).

- chlorite and talc-bearing eclogites (LSZ-06, LSZ-23 and LSZ-58)

Talc- (LSZ-06) and chlorite-bearing (LSZ-23; LSZ-58) eclogites randomly occur on the rims of Fe-Ti metagabbro blocks. They exhibit garnet crystals with two distinct generations intensively fractured and healed by a pyrope-rich garnet. Talc or chlorite (up to 10 vol.%) occur as elongated laths along the foliation between omphacite and garnet but have not been observed as inclusion within garnet cores. Talc-bearing domains are often associated with glaucophane shear bands and chlorite aggregates cutting across and postdating the mylonitic foliation.

Complex fracture patterns are found in the garnets. As an example, five successive tectono-metamorphic events were recorded by a single garnet grain from a chlorite-eclogite (sample LSZ-23; Fig. 6a,b). The boundary between garnet I and garnet II is lined by an embayment rich in Mn and Ca (respectively up to 10 mol. % and 25 mol. %). Pyrope content increases rimwards within garnet II, from c. 15 mol. % to 25 mol. %. Several "fossilized" fracture networks lined by a slightly Mg-enriched composition can also be identified (Fig. 6a,b).

5 Chemical variations in shear zones eclogites

Shear zones have been long recognized as a preferred locus for fluid-assisted mass transfer leading to bulk rock chemical alteration, as well as isotopic mixing (White and Knipe, 1978; Austrheim, 1987; Dipple and Ferry, 1992; Keller et al., 2004). In order to evaluate the degree of fluid circulation, the major element compositions of all rock-types encountered in the ISZ and LSZ were compared. The procedure used to obtain reliable compositions is given in Appendix B and detailed compositions are available in Supplementary material 4.

Figure 7a shows that low-strained and dry mylonitized Fe-Ti eclogites compositions (whether from the ISZ or the LSZ) plot in the middle of the ACF diagram. "Dry" mylonitized Fe-Ti metagabbros generally have a bulk composition which lies very close to the Lago Superiore area eclogites studied by Schwartz et al. (2000). By contrast, lawsonite-rich hydrated eclogites (dominantly cropping out in the LSZ) exhibit a striking depletion in FeO (-8 wt. %; Fig. 7a). This feature is also observed for lawsonite and omphacite-bearing veins sampled between brecciated fragments, whose composition largely differs from that of the undeformed Fe-Ti metagabbro (Fig. 7a).

Mg-chlorite and talc-bearing mylonites, where pseudomorphed lawsonite has not been observed, are significantly enriched in MgO: talc-bearing mylonites range from 9 to 16 wt.% MgO (Fig. 7a; low strained Fe-Ti metagabbros typically contain 6 wt.% MgO). Similar bulk rock

estimates for the phengite-bearing Fe-Ti metagabbro (LSZ-42) show that the K_2O bulk rock content of this sample is close to 1.5 wt.%, *i.e.* more than 5 times higher than the average K_2O content of Monviso Fe-Ti metagabbros (see Lombardo et al., 1978 and Schwartz et al., 2000).

A striking depletion in FeO is also recorded by garnet rims from LSZ eclogites (Fig. 7b), which are systematically depleted in almandine content, and corresponds to the transition between GrtI and GrtII (Fig. 6a). Garnet rim values for all samples are surprisingly similar (Fig. 7b) and generally trend towards 55% of almandine content. Such a trend is absent from the ISZ (and USZ) samples (Fig. 7b).

6. DISCUSSION

6.1 Petrological evolution during shear zone activity at 80 km depth

Our data (field relationships and petrography, mineralogy, chemical trends) suggest that eclogite-facies deformation of Fe-Ti metagabbros and fluid infiltration led to the formation of various mylonite types. Their relative timing of formation is presented in figure 8a and set back against P-T conditions (taken from Angiboust et al., 2011). We stress that the four steps described in figure 8a successively took place between 70 and 80 km depth under lawsonite eclogite facies conditions, as testified by the presence of lawsonite pseudomorphs all along the textural evolution (as porphyroblasts and/or in veins). Steps 2 to 4 occurred in a relatively narrow P-T range as demonstrated by similar thermobarometric estimates obtained on these texturally different assemblages (detailed calculations given in Angiboust et al., 2011).

“Dry” mylonites (Fig.8a-step2) are common along the ISZ and also occur in the LSZ. By contrast, the presence in the LSZ of strongly hydrated parageneses and extensive bulk rock alteration demonstrates that the blocks of Fe-Ti metagabbros dispersed along this shear zone recrystallized in a much more fluid-rich environment. Chemical data (Fig. 7a,b) indicate

contrasting degrees of bulk rock alteration, ranging from slightly (in the ISZ) to strongly altered (in the LSZ). Similarities in terms of rock types, P-T conditions and textures (garnet zoning and brecciation; lawsonite pseudomorphs) between the ISZ and LSZ suggest that the LSZ recorded a broadly coeval (i.e., at the same depths) yet slightly longer tectonic history than the ISZ, with marked fluid and mass transfer. This is consistent with the much more intense fragmentation of eclogite blocks and the larger spatial extension of the LSZ in the field (Figs. 2a, 3b,c). These additional stages of deformation and fluid influx, mostly recorded in the LSZ, are shown in figure 8a, as steps 3 (compare with Figs. 3e-f) and 4 (compare with Fig. 4d).

We finally point out that the presence of eclogitic breccias (Fig. 3e), garnet fractures (Fig. 6a) and block boudinage (Fig. 4d) attests to switches between brittle and ductile deformation, as shown in steps 2 through 4 (Fig. 8a). In the following sections, we use this petro-tectonic evolution to provide critical information on deformation patterns, fluid-rock interactions and rheological processes occurring within the eclogitized oceanic lithosphere, down dip in the subduction zone.

6.2 Contrasting ranges of fluid flow

The above data suggest a contrasting amount of fluid flow for the ISZ and the LSZ (Figure 8b), whose spatial extent is further discussed here.

The detailed analysis of ISZ garnets shows a complex zoning pattern (overgrowths, oscillations; Fig. 5f, supplementary material 2; see also Spandler et al., 2011), suggesting chemical system opening and deformation-assisted fluid circulation. Manganese, which is strongly partitioned within garnet cores, may have been dissolved during fracturing of garnet cores and subsequently precipitated after advective transport (for examples of garnet embayment within an ISZ eclogite, see Angiboust et al., 2011; their Fig. 3g). However, undeformed Fe-Ti

metagabbros and "dry" ISZ mylonite samples are chemically indistinguishable (Fig. 7a). Moreover, garnet rim almandine content from ISZ Fe-Ti eclogites is similar to that of undeformed, unaltered samples (Fig. 7b). Even if a very local infiltration of external fluid is possible (Spandler et al., 2011), our results support the predominance of relatively short range (i.e. meter-scale) fluid flow along the ISZ, as first inferred for Lago Superiore area eclogite mylonites from the presence of omphacitic crack-seal veins (e.g., Philippot and Selverstone, 1991; Nadeau et al., 1993; Table 1; Fig. 7a). Sharp interfaces between (omphacite filled) tensile cracks and mylonitized wall rock also suggest short-lived, incremental fluid-rock interaction and short vein lifetime (Philippot and Van Roermund, 1992).

In the LSZ, by contrast, our data point to larger-scale fluid flow and substantial metasomatism (Fig. 7a; with noticeable chemical potential gradients in H_2O, SiO_2 and FeO; e.g., Ferry, 1979) between the serpentinite matrix and the blocks of Fe-Ti metagabbros (see Fig. 8a, steps 3-4). Dissolution figures and associated overgrowths (Figs. 6a,c) show that the garnet surface was successively enriched in Mn-Ca then in Mg. This sharp boundary between Grt I and Grt II in LSZ eclogites (Figs. 6a,c; Fig.7b) requires the advection of elements (and chemical system opening) close to peak conditions. The decrease of garnet almandine content within core-rim profiles for all LSZ samples towards a similar value (Fig. 7b) strongly suggests a buffering and input of Mg by the adjacent thick serpentinite sole (Figs. 2b,3b).

Eclogite porosity is generally limited to microfractures, isolated pores, cleavage planes and mineral boundaries (e.g. Mibe et al., 2003), connectivity is presumably very limited (Watson and Brenan, 1987; Davies, 1999) and eclogite permeability is estimated at six orders of magnitude lower than for serpentinite mylonites ($10^{-18}m^2$; Morrow et al., 1984). We thus suggest that serpentinite-bearing shear zones, particularly the LSZ, acted as true conduits for fluid flow, despite the fact that the relatively low permeability of the blocks possibly deflected most of the flow through the matrix and limited deep infiltration into the blocks (Ague, 2007).

Whether fluids channelized within the LSZ originate from antigorite breakdown (which occurs close, yet slightly deeper than estimated peak conditions: ~650°C, 25-30kbar; Scambelluri et al., 1995; Ulmer and Trommsdorff, 1995) or derive from dehydration of the adjacent Mg-Al gabbro body during prograde reactions remains uncertain (see also the discussion on ISZ veins by Spandler et al., 2011). Chemical exchange and the formation of metasomatic rinds in any case facilitated the transposition of fabrics and enhanced fragment disaggregation, as observed on the block rims along the LSZ (Fig. 3c; for similar blackwall examples: Bebout and Barton, 2002; Catlos and Sorensen, 2003; Breeding et al., 2004).

6.3 Rheology of the subducting lithosphere and strain localization at depth

The Lago Superiore Unit provides a unique opportunity to document deep deformation processes occurring in subducted oceanic lithosphere, from the kilometer scale to the mineral scale, and to compare it with theoretical rheological parameters derived from rock flow laws based on experimental data (e.g., Kirby, 1983).

6.3.1 Rheological behaviour at the kilometer scale

Bulk cumulative strain inferred from field observations is shown in figure 9b (and set back against the cross-section of figure 9c). This profile shows that the main shear zones are preferentially located along the major lithological contrasts, i.e. at the boundary between materials with significantly different strengths and viscosities. In agreement with theoretical studies of multilayered media (e.g., Stromgard, 1973; Treagus, 1981), this confirms that interfaces between rocks with different competencies are the loci of maximized shear strain.

For the sake of comparison, we tentatively evaluated the strength of each layer of the column using available dislocation creep flow laws for similar materials (Fig. 9a). This profile has

been calculated using a constant strain rate of 10^{-14} s^{-1}. Other details of the calculation method are given in Appendix C. Our field observations (Fig. 9b) qualitatively strengthen the rheological envelope inferred from laboratory experiments (Fig. 9a) in showing that gabbros are indeed stronger than the overlying metabasaltic sequence under peak conditions (in agreement with preliminary observations; Burg and Philippot, 1991). However, the geometry of the whole system (stack of layers) implies that the different shear zones were active for the same range of shear stresses, a statement at variance with the very large strength contrasts derived from dislocation creep flow laws (Fig. 9a). In particular, in spite of the presence of a thick serpentine sole supposedly so weak as to accommodate all the deformation, not only the shear zones (where serpentinite slivers are commonly found) but also the bulk of the metabasalt unit was pervasively deformed. This relative weakness of eclogites, not well reflected in experimental flow laws (Fig. 9a), could be related to their high water content, as rock strength is known to be significantly reduced by the presence of dissolved water ("hydrolytic weakening"; Griggs, 1967; Rybacki and Dresen, 2000; Zhang and Green, 2007), particularly within omphacite (whose H_2O content commonly reaches 1000 ppm in natural eclogites; e.g. Katayama et al., 2006).

Although ductile deformation dominates the deep evolution of this ophiolite, brittle deformation is apparent in veins (Fig. 5g) and in the breccia structures on the rims of the blocks of the LSZ (Fig 3c-e; Fig.4c). These observations are consistent with the experimental results describing a "semi-brittle" mode of deformation, in particular for clinopyroxene (Kirby and Kronenberg, 1984; Rutter, 1986; Philippot and Van Roermund, 1992). It should be noted that the "clasts" of these breccia are mylonite fragments, and that the whole breccia is generally reworked by ductile deformation, i.e., brecciation is bracketed by two phases of mylonitization (Fig. 8a, step4). Pseudotachylytes marking brittle rupture (Austrheim and Boundy, 1994; Andersen and Austrheim, 2006) have not been observed within the Lago Superiore Unit, despite extensive investigations. This could be due to the fact that pseudotachylites preferentially develop in

extremely water-poor protoliths (John et al., 2009), whereas the Lago Superiore Unit shear zones show ample evidence for abundant fluid circulation.

6.3.2 At the cm-scale: phase segregation and garnet fracturing

Phase segregation between omphacite and garnet (Fig. 3d, Fig. 4d, Fig. 8a-step 2) was described in shear zones from the Tauern, Dabie Sulu, Caledonides (Holland, 1979; Ji et al., 2003; Terry and Heidelbach, 2006) and in experimentally deformed eclogites under high shear strain (Zhang and Green, 2007), but at temperatures much higher than those reported for Lago Superiore eclogites. Mechanisms invoked for phase segregation include mineral reactions, deformation-related processes such as dynamic recrystallization associated with grain size reduction (Philippot and Van Roermund, 1992; Mauler et al., 2000; Terry and Heidelbach, 2006) and/or the presence of a free fluid phase (e.g., Essene and Fyfe, 1967; Holland, 1979; Schliestedt, 1990; Selverstone et al., 1992).

We suggest that the segregation of garnet (otherwise behaving as rotating rigid spheres in a matrix of weaker omphacite) into lenses or layers may well explain their fracturing (Fig. 8b) as a result of indentation at garnet-to-garnet contacts. This does not preclude the contribution of other processes, such as hydraulic fracturing (Spandler et al., 2011), but does not require the presence of a very high pore fluid pressure. In principle, with increasing strain such angular fragments can be disseminated along the foliation by cataclastic flow (e.g., Tullis and Yund, 1987). This is locally observed in some very dry eclogite mylonites along the ISZ (ISZ-49; Fig.2a), but most garnet fractures, within both ISZ and LSZ samples, are healed without evidence of relative displacement (Fig. 5d, Fig. 6a). Fast healing of garnet requires efficient element mobility, which is fostered by a free fluid phase (Erambert and Austrheim, 1993) and by grain size reduction (Rutter and Brodie, 1995). The preservation of an almost undisturbed garnet I shape at the core of garnet II also suggests the existence of a stress drop after fracturing (Fig. 6d), since garnet fragments would

otherwise have been disseminated by ongoing strain. This result is consistent with the very large minimum stress drops associated with very small earthquakes, inferred from pseudotachylytes of Corsica (Andersen et al., 2008). These observed deformation and growth patterns thus potentially relate to co-seismic deformation and intermediate-depth coupling processes (see also Erambert and Austrheim, 1993). On the other hand, phase segregation and healed fractures also point to a key contribution to small-scale deformation processes from dissolution-precipitation, in addition to creep. Dissolution-precipitation may indeed be an important deformation mechanism within omphacite-rich domains, which are particularly subject to channelized fluid circulation (Piepenbreier and Stöckhert, 2001), or within garnets (as shown by the propagation of crack-tips; Prior, 1993).

6.4 Implications for km-scale, geodynamic processes at the subduction interface

Our results demonstrate that the Lago Superiore ophiolite was affected by intense shearing dominantly accommodated along three major shear zones defined by eclogite-facies mylonites and/or serpentinite slivers (Fig. 8b). Lenses and blocks dispersed along these shear zones, as well as the whole of the Lago Superiore, display similar P-T conditions (Angiboust et al., 2011), suggesting spatially limited tectonic mixing. The error bar associated with the thermobarometric methods used here (i.e. ±20°C and ± 1.5 kbar) implies that less than c. 12 km of cumulative displacement occurred along these shear zones (considering a dip of 45° for the plate interface). The slightly hotter temperatures reported in a calcschist lens embedded within the LSZ (Fig. 3a; 560-570°C; Angiboust et al., 2011) may reflect the fact that the lower portion of the ophiolite reached slightly greater depths (≤ 3 km deeper) than the overlying portions of the Lago Superiore ophiolite (Fig. 10a). These shear zones, particularly the LSZ, represent an example of network widening (in the sense of Schrank et al., 2008, for example) and not a subduction mélange formed by extensive mixing along the subduction interface (Blake et al., 1995; Guillot et al., 2004). The

above description of deformation patterns within the Lago Superiore ophiolite thus suggests that caution is needed before interpreting former eclogite-facies shear zones as serpentinite mélanges, particularly in areas with limited surface exposures (e.g., Voltri; Brouwer et al., 2002; Federico et al., 2007).

We emphasize that mylonitized Fe-Ti metagabbros blocks found dispersed within serpentinite in the LSZ originate from the ISZ for two reasons: (i) the main source of Fe-Ti gabbros is structurally located at the top of the Mg-Al gabbroic body (Figs.3a, 8b) (ii) mylonitization of such eclogites cannot happen once the blocks are embedded within the rheologically much weaker serpentinite. Such Fe-Ti metagabbros thus constitute markers of the relative displacement along the shear zones. The blocks from the LSZ successively underwent mylonitization along the ISZ (Fig. 10a), shearing and detachment from the ISZ by a ball-bearing mechanism before being embedded in the serpentinites schists of the LSZ (Fig. 10b). Note that displacement of eclogitic blocks from ISZ to LSZ through the gabbroic body could have been facilitated by the presence of an inherited structural weakness (such as bending-related faults; e.g. Ranero et al., 2003), tectonically reactivated as a thrust during deep shearing.

The final detachment of the Lago Superiore ophiolitic slice as a whole implies that deformation migrated towards the base of the serpentinite sole (Fig. 10c). Strain localization within the ultramafic section of the lithosphere probably occurs at the transition between highly and midly serpentinized peridotite (i.e., at depths of a few hundred meters to a few km below the oceanic Moho; Minshull et al., 1998; Iyer et al., 2010). It is likely that from this stage onwards (Fig. 10c) both the ISZ and LSZ were less active, and consequently preserved from extensive overprinting.

The behaviour of the Lago Superiore ophiolite after detachment remains somewhat speculative but is closely linked (as discussed by Agard et al., 2009) with the upward, buoyancy-driven exhumation of light continental material (ρ~2700kg.m^{-3}) dragging these dense (ρ=3300-3400kg.m^{-3}; *e.g.* Stern, 2004; Lapen et al., 2007; Angiboust and Agard, 2010) portions of

eclogitized oceanic lithosphere along the subduction interface. Accordingly, younger peak ages recorded in the adjacent, continental Dora Maira internal crystalline massif (c. 35-40 Ma v. 40-45 Ma for Monviso; Tilton et al., 1991; Duchêne et al., 1997; Rubatto and Hermann, 2001) would imply that the ophiolite remained at depth for ~5 My before being dragged upwards by the Dora Maira unit. In the meantime, the Lago Superiore slice may have remained buoyant enough thanks to the buoyant serpentinite sole at the base of the section (300-500m; ρ=2900 kg.m^{-3}; Schwartz et al., 2001; Guillot et al., 2004) and/or to the overall fluid content in the mafic section (Angiboust and Agard, 2010). Further geochronological data are now required to better constrain the relative timing of deformation and deep thrusting processes responsible for detachment and exhumation of the Monviso ophiolite and its relationships with the underlying Dora Maira unit.

6. **Conclusions**

The Lago Superiore Unit, which exposes a very well-preserved lithospheric-scale tectonic ophiolitic slice returned from c. 80 km depth in the Alpine subduction zone, is crosscut by a network of three km-scale shear zones. It therefore provides a unique opportunity to study strain localization and rheological weakening in the subducting lithosphere. Our results show that:

(i) Strain was strongly localized within eclogite-facies shear zones at the interface between layers presenting rheological contrasts (i.e. between basalts, gabbros and serpentinites).

(ii) Dominantly short-range fluid flow occurred at the basalt-gabbro boundary (ISZ) through repeated fracturing processes associated with mylonitization of the shear zone. By contrast, we identified a longer-lived, pervasive deformation-enhanced fluid pathway at the gabbro-serpentinite interface (LSZ) leading to strong metasomatism, mechanical weakening and dismembering of the block fragments within serpentinite schists.

(iii) The presence of eclogite "breccias", preserving numerous healed fractured garnet crystals, suggest a local brittle behaviour of the oceanic crust, possibly associated with co-seismic deformation.

(iv) The activity of both the ISZ and LSZ stopped during early lawsonite eclogite-facies exhumation when deformation localized deeper within the serpentinite sole, allowing for the detachment (and preservation) of this large ophiolitic fragment.

Appendix A

Analytical methods:

Mineral abbreviations used in this work are after Whitney and Evans (2010).

The mineral analyses were performed using a Cameca SX100 electron microprobe (Camparis, Univ. Paris 6; a Cameca SX50 was also used for additional conventional analyses). Classical analytical conditions were adopted for spot analyses [15 kV, 10 nA, wavelength-dispersive spectroscopy (WDS) mode], using Fe_2O_3 (Fe), $MnTiO_3$ (Mn, Ti), diopside (Mg, Si), CaF_2 (F), orthoclase (Al, K), anorthite (Ca) and albite (Na) as standards. Chemical maps of garnet were obtained at the SX100 electron microprobe using 15 kV, 20 nA and a counting time of 100ms. Quantifications were derived from the automated Cameca ZAF quantification procedure.

Chemical composition of microdomains (~3mm x 1.5mm) studied for bulk rock composition analysis were obtained at the Geology Laboratory of the Ecole Normale Supérieure (Paris) using a Zeiss Sigma field-emission-gun SEM with an X-max Oxford detector (50 mm^2), an acceleration voltage of 20 kV and a counting time of 1 minute per domain.

Three additional whole-rock chemical analyses were undertaken at the SARM (CRPG Nancy) from c. 5 cm^3 of each representative rock sample (ISZ-17, sole-55 and LSZ-18-2). The major elements were analysed by inductively coupled plasma-optical emission (ICP-OES) spectroscopy after fusion with $LiBO_3$ and dissolution in HNO_3. More details on the method are given in Carignan et al. (2001). H_2O content was determined by loss on ignition.

Appendix B

Bulk rock composition analysis:

Chemical composition of fifteen thin sections from USZ, ISZ and LSZ were calculated either by averaging of several surface compositions scans using a FEG-SEM (average between 2 and 5 surface analyses) or by a combination of visual percentage estimated modes (Terry and Chilingar, 1955) and averaged EMP chemical analyses. Detailed chemical compositions, average values and sampling GPS coordinates are given in Supplementary material 4.

Appendix C

Construction of the rheological profile

In order to compare rheological properties of the materials, fixed value of 10^{-14} s^{-1} has been chosen for the calculation. Note that integrated strain rates for subduction zones, generally between 10^{-13} and 10^{-14} s^{-1} may be substantially higher along shear zones (between 10^{-9} and 10^{-12} s^{-1}; Sibson, 1986; Stöckhert, 2002; Burg and Gerya, 2005), leading to significant increase of rock strength and a marked decrease of rock viscosity

For the basaltic upper section (Fig.9a), we use an omphacite power law creep rheology (Zhang, 2006) to describe its behaviour because omphacite appears to be the dominant (c. 75%) mineral under eclogite-facies conditions. This assumption is justified by the fact that garnet (less than 15 vol.% in the eclogitized basaltic crust) does not exhibit a strong fabric and generally behaves as a rotating rigid body during plastic deformation of eclogite (e.g. Mainprice et al., 2004). For Fe-Ti

metagabbros, where the relative amount of garnet locally reaches 40 vol.%, an eclogite flow law is considered to be more appropriate (Jin et al., 2001). We also consider that Mg-Al gabbro is rheologically similar to diabase, whose mineralogy is also composed of a Ca-rich plagioclase and clinopyroxene (Mackwell, 1995). As Fe-Ti metagabbros are included in the uppermost portion of the Mg-Al metagabbro, the whole gabbroic unit is believed to behave as a coherent body (Fig. 9). Serpentinite exhibits a viscosity which is over 4 orders of magnitude lower than metagabbros (following the flow law for antigorite from Hilairet et al., 2007).

Experimental parameters for the eclogite flow law (calculated for 50% garnet, 40% omphacite, and 10% quartz; Jin et al., 2001) yield an unrealistic rock strength of 7 GPa for Fe-Ti metagabbros under these relatively cold conditions (T=550°C; Fig. 9a). This value will likely be lowered in our samples since garnet, considered as responsible for strengthening of the eclogites in the dislocation creep regime (Jin et al., 2001) represents only 25–30 vol.%. Pervasive ductile deformation of metagabbros contrasts with the presence of omphacite-bearing crack-seal veins (earlier reported in eclogite-facies mylonites from the Lago Superiore Area; Philippot, 1987), which constitute one of the rare examples attesting to local brittle behaviour of oceanic crust under HP-LT conditions.

Acknowledgements

We acknowledge Loïc Labrousse, Dave Waters, Anne Verlaguet, Laetitia Le Pourhiet and Alexandre Schubnel for insightful remarks and discussions. Ryan Langdon, Christian Chopin and Alexandre Dimanov are thanked for technical assistance. This paper benefited from thoughtful reviews from Jane Selverstone and Torgeir Andersen. Marco Scambelluri is acknowledged for careful reading and editorial handling. This work has been funded with an INSU grant to P.A.

References

Abers, G.A., van Keken, P.E., Kneller, E.A., Ferris, A., Stachnik, J.C., 2006. The thermal structure of subduction zones constrained by seismic imaging: Implications for slab dehydration and wedge flow. Earth and Planetary Science Letters 241(3-4), 387-397.

Agard, P., Jolivet, L., Goffé, B., 2001. Tectonometamorphic evolution of the Schistes Lustre's complex: implications for the exhumation of HP and UHP rocks in the western Alps. Bulletin De La Societe Geologique De France 172(5), 617-636.

Agard, P., Monie, P., Jolivet, L., Goffé, B., 2002. Exhumation of the Schistes Lustres complex: in situ laser probe Ar-40/Ar-39 constraints and implications for the Western Alps. Journal of Metamorphic Geology 20(6), 599-618.

Agard, P., Yamato, P., Jolivet, L., Burov, E., 2009. Exhumation of oceanic blueschists and eclogites in subduction zones: Timing and mechanisms. Earth-Science Reviews 92(1-2), 53-79.

Ague, J.J., 2007. Models of permeability contrasts in subduction zone mélange: Implications for gradients in fluid fluxes, Syros and Tinos Islands, Greece. Chemical Geology 239(3-4), 217-227.

Andersen, T.B., Austrheim, H., 2006. Fossil earthquakes recorded by pseudotachylytes in mantle peridotite from the Alpine subduction complex of Corsica. Earth and Planetary Science Letters 242(1-2), 58-72.

Andersen, T.B., Mair, K., Austrheim, H., Podladchikov, Y., Vrijmoed, J.C., 2008. Stress release in exhumed intermediate and deep earthquakes determined from ultramafic pseudotachylyte. Geology 36(12), 995-998.

Angiboust, S., Agard, P., 2010. Initial water budget: The key to detaching large volumes of eclogitized oceanic crust along the subduction channel? Lithos 120, 453-474.

Angiboust, S., Agard, P., Jolivet, L., Beyssac, O., 2009. The Zermatt-Saas ophiolite: the largest (60-km wide) and deepest (c. 70-80km) continuous slice of oceanic lithosphere detached from a subduction zone? Terra Nova 21, 171-180.

Angiboust, S., Langdon, R., Agard, P., Waters, D., Chopin, C., 2011. Eclogitization of the Monviso ophiolite and implications on subduction dynamics. Journal of Metamorphic Geology, in press.

Audet, P., Bostock, M.G., Christensen, N.I., Peacock, S.M., 2009. Seismic evidence for overpressured subducted oceanic crust and megathrust fault sealing. Nature 457(7225), 76-78.

Austrheim, H., 1987. Eclogitization of lower crustal granulites by fluid migration through shear zones. Earth and Planetary Science Letters 81(2-3), 221-232.

Austrheim, H., Andersen, T.B., 2004. Pseudotachylytes from Corsica: fossil earthquakes from a subduction complex. Terra Nova 16(4), 193-197.

Austrheim, H., Boundy, T.M., 1994. Pseudotachylytes Generated During Seismic Faulting and Eclogitization of the Deep Crust. Science 265(5168), 82-83.

Bachmann, R., Glodny, J., Oncken, O., Seifert, W., 2009. Abandonment of the South Penninic-Austroalpine palaeosubduction zone, Central Alps, and shift from subduction erosion to accretion: constraints from Rb/Sr geochronology. Journal of the Geological Society 166(2), 217-231.

Ballèvre, M., Lagabrielle, Y., Merle, O., 1990. Tertiary ductile normal faulting as a consequence of lithospheric stacking in the western Alps. Deep structure of the Alps. Societe Geologique de France 156, 227–236.

Bearth, P., 1967. Die Ophiolite der zone von Zermatt-Saas Fee. Materiaux pour la Carte Geologique de la Suisse, Neue Folge 132, 1-130.

Bebout, G.E., Barton, M.D., 2002. Tectonic and metasomatic mixing in a high-T, subduction-zone mélange--insights into the geochemical evolution of the slab-mantle interface. Chemical Geology 187(1-2), 79-106.

Beltrando, M., Rubatto, D., Manatschal, G., 2010. From passive margins to orogens: The link between ocean-continent transition zones and (ultra)high-pressure metamorphism. Geology 38(6), 559-562.

Blake Jr, M.C., Moore, D.E., Jayko, A.S., 1995. The role of serpentinite melanges in the unroofing of ultrahigh-pressure metamorphic rocks: An example from the Western Alps. Ultrahigh pressure metamorphism, Cambridge University Press, 182–205 pp.

Blake, M.C., Jayko, A.S., 1990. Uplift of very high pressure rocks in the western Alps: evidence for structural attenuation along low-angle faults. Mémoire de la Société Géologique de France 156, 237-246.

Boundy, T.M., Fountain, D.M., Austrheim, H., 1992. Structural development and petrofabrics of eclogite facies shear zones, Bergen Arcs, western Norway: implications for deep crustal deformational processes. Journal of Metamorphic Geology 10(2), 127-146.

Breeding, C.M., Ague, J.J., Bröcker, M., 2004. Fluid-metasedimentary rock interactions in subduction-zone mélange: Implications for the chemical composition of arc magmas. Geology 32(12), 1041-1044.

Brouwer, F.M., Vissers, R.L.M., Lamb, W.M., 2002. Metamorphic history of eclogitic metagabbro blocks from a tectonic mélange in the Voltri massif, Ligurian Alps, Italy. Ofioliti 27(1), 1-16.

Burg, J.P., Gerya, T.V., 2005. The role of viscous heating in Barrovian metamorphism of collisional orogens: thermomechanical models and application to the Lepontine Dome in the Central Alps. Journal of Metamorphic Geology 23(2), 75-95.

Burg, J.-P., Philippot, P., 1991. Asymmetric compositional layering of syntectonic metamorphic veins as way-up criterion. Geology 19(11), 1112-1115.

Carignan, J., Hild, P., Mevelle, G., Morel, J., Yeghicheyan, D., 2001. Routine Analyses of Trace Elements in Geological Samples using Flow Injection and Low Pressure On-Line Liquid Chromatography Coupled to ICP-MS: A Study of Geochemical Reference Materials BR, DR-N, UB-N, AN-G and GH. Geostandards Newsletter 25(2-3), 187-198.

Castelli, D., Rostagno, C., Lombardo, B., 2002. Jd-Qtz-bearing metaplagiogranite from the Monviso meta-ophiolite (Western Alps). Ofioliti 27, 81-90.

Catlos, E.J., Sorensen, S.S., 2003. Phengite-Based Chronology of K- and Ba-Rich Fluid Flow in Two Paleosubduction Zones. Science 299(5603), 92-95.

Cliff, R.A., Barnicoat, A.C., Inger, S., 1998. Early Tertiary eclogite facies metamorphism in the Monviso Ophiolite. Journal of Metamorphic Geology 16(3), 447-455.

Compagnoni, R., Rolfo, F., Manavella, F., Salusso, F., 2007. Jadeitite in the Monviso meta-ophiolite, Piemonte Zone, Italian western Alps. Periodico di Mineralogia 76(2), 79-89.

Coward, M., Dietrich, D., 1989. Alpine tectonics - an overview. Geological Society, London, Special Publications 45(1), 1-29.

Dal Piaz, G.V., Hunziker, J.C., Martinotti, G., 1972. La Zona Sesia-Lanzo e l'evoluzione tettonino-metamorphica delle Alpi nordoccidentali interne. Mem. Societa. Geologica Italiana. Roma, 11, 433-472.

Davies, J.H., 1999. The role of hydraulic fractures and intermediate-depth earthquakes in generating subduction-zone magmatism. Nature 398(6723), 142-145.

Deville, E., Fudral, S., Lagabrielle, Y., Marthaler, M., Sartori, M., 1992. From oceanic closure to continental collision: A synthesis of the "Schistes lustrés" metamorphic complex of the Western Alps. Geological Society of America Bulletin 104(2), 127-139.

Dipple, G.M., Ferry, J.M., 1992. Metasomatism and fluid flow in ductile fault zones. Contributions to Mineralogy and Petrology 112(2), 149-164.

Duchene, S., Lardeaux, J.M., Albarede, F., 1997. Exhumation of eclogites: insights from depth-time path analysis. Tectonophysics 280(1-2), 125-140.

Erambert, M., Austrheim, H., 1993. The effect of fluid and deformation on zoning and inclusion patterns in poly-metamorphic garnets. Contributions to Mineralogy and Petrology 115(2), 204-214.

Essene, E.J., Fyfe, W.S., 1967. Omphacite in Californian metamorphic rocks. Contributions to Mineralogy and Petrology 15(1), 1-23.

Federico, L., Crispini, L., Scambelluri, M., Capponi, G., 2007. Ophiolite melange zone records exhumation in a fossil subduction channel. Geology 35(6), 499-502.

Fountain, D.M., Boundy, T.M., Austrheim, H., Rey, P., 1994. Eclogite-facies shear zones--deep crustal reflectors? Tectonophysics 232(1-4), 411-424.

Gerya, T.V., Stockhert, B., Perchuk, A.L., 2002. Exhumation of high-pressure metamorphic rocks in a subduction channel: A numerical simulation. Tectonics 21(6), 6-1 .

Griggs, D., 1967. Hydrolytic Weakening of Quartz and Other Silicates*. Geophysical Journal of the Royal Astronomical Society 14(1-4), 19-31.

Groppo, C., Castelli, D., 2010. Prograde P-T evolution of a lawsonite eclogite from the Monviso metaophiolite (Western Alps): dehydration and redox reactions during subduction of oceanic FeTI-oxide gabbro. Journal of Petrology 51(12), 2489-2514.

Guillot, S., Schwartz, S., Hattori, K., Auzende, A., Lardeaux, J., 2004. The Monviso ophiolitic Massif (Western Alps), a section through a serpentinite subduction channel. Evolution of the western Alps : insights from metamorphism, structural geology, tectonics and geochronology, The Virtual Explorer: pp. Paper 3.

Handy, M.R., Wissing, S.B., Streit, L.E., 1999. Frictional-viscous flow in mylonite with varied bimineralic composition and its effect on lithospheric strength. Tectonophysics 303(1-4), 175-191.

Hattori, K.H., Guillot, S., 2007. Geochemical character of serpentinites associated with high- to ultrahigh-pressure metamorphic rocks in the Alps, Cuba, and the Himalayas: Recycling of elements in subduction zones. Geochemistry Geophysics Geosystems 8(9), Q09010.

Healy, D., Reddy, S.M., Timms, N.E., Gray, E.M., Brovarone, A.V., 2009. Trench-parallel fast axes of seismic anisotropy due to fluid-filled cracks in subducting slabs. Earth and Planetary Science Letters 283(1-4), 75-86.

Hermann, J., Müntener, O., Scambelluri, M., 2000. The importance of serpentinite mylonites for subduction and exhumation of oceanic crust. Tectonophysics 327(3-4), 225-238.

Hilairet, N. et al., 2007. High-Pressure Creep of Serpentine, Interseismic Deformation, and Initiation of Subduction. Science 318, 1910.

Holland, T., 1979. High water activity in the generation of high-pressure kyanite eclogite of the Tauern window, Austria. Journal of Geology 87, 1-27.

Ikesawa, E., Sakaguchi, A., Kimura, G., 2003. Pseudotachylyte from an ancient accretionary complex: Evidence for melt generation during seismic slip along a master decollement? Geology 31(7), 637-640.

Iyer, K., Rüpke, L.H., Morgan, J.P., 2010. Feedbacks between mantle hydration and hydrothermal convection at ocean spreading centers. Earth and Planetary Science Letters 296(1-2), 34-44.

Ji, S. et al., 2003. Microstructures, petrofabrics and seismic properties of ultra high-pressure eclogites from Sulu region, China: implications for rheology of subducted continental crust and origin of mantle reflections. Tectonophysics 370(1-4), 49-76.

Jin, Z.M., Zhang, J., Green, H.W., Jin, S., 2001. Eclogite rheology: Implications for subducted lithosphere. Geology 29(8), 667-670.

John, T. et al., 2009. Generation of intermediate-depth earthquakes by self-localizing thermal runaway. Nature Geosciences 2(2), 137-140.

John, T., Schenk, V., 2006. Interrelations between intermediate-depth earthquakes and fluid flow within subducting oceanic plates: Constraints from eclogite facies pseudotachylytes. Geology 34(7), 557-560.

Katayama, I., Nakashima, S. and Yurimoto, H., 2006. Water content in natural eclogite and implication for water transport into the deep upper mantle. Lithos 86(3-4), 245-259.

Keller, L.M., Abart, R., Stünitz, H., De Capitani, C., 2004. Deformation, mass transfer and mineral reactions in an eclogite facies shear zone in a polymetamorphic metapelite (Monte Rosa nappe, western Alps). Journal of Metamorphic Geology 22(2), 97-118.

Kirby, S.H., 1983. Rheology of the lithosphere. Reviews in Geophysics 21(6), 1458-1487.

Kirby, S.H., 1985. Rock mechanics observations pertinent to the rheology of the continental lithosphere and the localization of strain along shear zones. Tectonophysics 119(1-4), 1-27.

Kirby, S.H., Kronenberg, A.K., 1984. Deformation of Clinopyroxenite: Evidence for a Transition in Flow Mechanisms and Semibrittle Behavior. Journal of Geophysical Research 89(B5), 3177-3192.

Lagabrielle, Y., Cotten, J., 1984. Le matériel détritique ophiolitique des séries océaniques liguro-piémontaises. L'exemple du Haut Queyras. Contribution à l'étude des prasinites. Ofioliti 9, 43-66.

Lagabrielle, Y., Lemoine, M., 1997. Alpine, Corsican and Apennine ophiolites: the slow-spreading ridge model. Comptes Rendus de l'Académie des Sciences - Series IIA - Earth and Planetary Science 325(12), 909-920.

Lapen, T. et al., 2007. Coupling of oceanic and continental crust during Eocene eclogite-facies metamorphism: evidence from the Monte Rosa nappe, western Alps. Contributions to Mineralogy and Petrology 153, 139-157.

Lardeaux, J.-M., Caron, J.-M., Nisio, P., Péquignot, G., Boudeulle, M., 1986. Microstructural criteria for reliable thermometry in low-temperature eclogites. Lithos 19(3-4), 187-203.

Lombardo, B. et al., 1978. Osservazioni preliminari sulle ofioliti metamorfiche del Monviso (Alpi occidentali). Rendiconti Societa Italiana Mineralogia Petrologia 34, 253-305.

Mackwell, S., Zimmermann, M., Kohlestdt, D., Scherber, D., 1995. Experimental deformation of dry Columbia diabase: implications for tectonics of Venus. Rock mechanics: proceedings of the 35th U.S. Symposium, University of Nevada: J.Daemen, R. Schultz Editors; Reno/5-7 June 1995.

Mainprice, D., Bascou, J., Cordier, P., Tommasi, A., 2004. Crystal preferred orientations of garnet: comparison between numerical simulations and electron back-scattered diffraction (EBSD) measurements in naturally deformed eclogites. Journal of Structural Geology 26(11), 2089-2102.

Martin, L.A.J., Ballèvre, M., Boulvais, P., Halfpenny, A., Vanderhaeghe, O., Duchêne, S., Deloule, E., 2011. Garnet re-equilibration by coupled dissolution–reprecipitation: evidence from textural, major element and oxygen isotope zoning of 'cloudy' garnet. Journal of Metamorphic Geology 29(2), 213-231.

Mauler, A., Burlini, L., Kunze, K., Philippot, P., Burg, J.P., 2000. P-wave anisotropy in eclogites and relationship to the omphacite crystallographic fabric. Physics and Chemistry of the Earth, Part A: Solid Earth and Geodesy 25(2), 119-126.

Meneghini, F., Di Toro, G., Rowe, C.D., Moore, J.C., Tsutsumi, A., Yamagushi, A.,, 2010. Record of mega-earthquakes in subduction thrusts: The black fault rocks of Pasagshak Point (Kodiak Island, Alaska). Geological Society of America Bulletin 122(7-8), 1280-1297.

Messiga, B., Kienast, J.R., Rebay, G., Riccardi, M.P., Tribuzio, R., 1999. Cr-rich magnesiochloritoid eclogites from the Monviso ophiolites (Western Alps, Italy). Journal of Metamorphic Geology 17(3), 287-299.

Mibe, K., Yoshino, T., Ono, S., Yasuda, A., Fujii, T., 2003. Connectivity of aqueous fluid in eclogite and its implications for fluid migration in the Earth's interior. Journal of Geophysical Research 108(B6), 2295.

Minshull, T.A., Muller, M.R., Robinson, C.J., White, R.S., Bickle, M.J., 1998. Is the oceanic Moho a serpentinization front? Geological Society of London, Special Publications 148(1), 71-80.

Monié, P., Philippot, P., 1989. Mise en évidence de l'âge éocène moyen du métamorphisme de haute pression dans la nappe ophiolitique du Monviso (Alpes Occidentales) par la méthode 39 Ar---40 Ar. Comptes Rendus de l'Academie des Sciences 309, 245–251.

Montési, L.G.J., Hirth, G., 2003. Grain size evolution and the rheology of ductile shear zones: from laboratory experiments to postseismic creep. Earth and Planetary Science Letters 211(1-2), 97-110.

Monviso, 1980. The Monviso ophiolite complex. Extract from "Ophiolites: Proceedings International Ophiolite Symposium", Cyprus 1979, 332-340.

Morrow, C.A., Shi, L.Q., Byerlee, J.D., 1984. Permeability of Fault Gouge Under Confining Pressure and Shear Stress. Journal of Geophysical Research 89(B5), 3193-3200.

Nadeau, S., Philippot, P., Pineau, F., 1993. Fluid inclusion and mineral isotopic compositions (HCO) in eclogitic rocks as tracers of local fluid migration during high-pressure metamorphism. Earth and Planetary Science Letters 114(4), 431-448.

Oberhänsli, R., Goffé, B., 2004. Metamorphic Structure of the Alps. C.C.G.M Paris.

Oncken, O., and ANCORP working group, 2003. Seismic imaging of a convergent continental margin and plateau in the central Andes (Andean Continental Research Project 1996 (ANCORP'96)). Journal of Geophysical Research. 108(B7), 2328.

Philippot, P., 1987. Crack-seal vein geometry in eclogitic rocks. Geodinamica acta 3, 171-181.

Philippot, P., Kienast, J.-R., 1989. Chemical-microstructural changes in eclogite-facies shear zones (Monviso, Western Alps, north Italy) as indicators of strain history and the mechanism and scale of mass transfer. Lithos 23(3), 179-200.

Philippot, P., Selverstone, J., 1991. Trace-element-rich brines in eclogitic veins: implications for fluid composition and transport during subduction. Contributions to Mineralogy and Petrology 106(4), 417-430.

Philippot, P., van Roermund, H.L.M., 1992. Deformation processes in eclogitic rocks: evidence for the rheological delamination of the oceanic crust in deeper levels of subduction zones. Journal of structural geology 14(8-9), 1059-1077.

Piepenbreier, D., Stöckhert, B., 2001. Plastic flow of omphacite in eclogites at temperatures below 500°C - implications for interplate coupling in subduction zones. International Journal of Earth Sciences 90(1), 197-210.

Platt, J.P., Behr, W.M., 2011. Lithospheric shear zones as constant stress experiments. Geology 39(2), 127-130.

Pognante, U., Kienast, J.-R., 1987. Blueschist and Eclogite transformations in Fe-Ti Gabbros: A Case from the Western Alps Ophiolites. Journal of Petrology 28(2), 271-292.

Polino, R., Dal Piaz, GV. And Guido, G., 1990. Tectonic erosion at the Adria margin and accretionnary processes for the Cretaceous orogeny of the Alps. Mémoire de la Société Géologique de France 156, 345-367.

Prior, D.J., 1993. Sub-critical fracture and associated retrogression of garnet during mylonitic deformation. Contributions to Mineralogy and Petrology 113(4), 545-556.

Raimbourg, H., Jolivet, L., Leroy, Y., 2007. Consequences of progressive eclogitization on crustal exhumation, a mechanical study. Geophysical Journal International 168(1), 379-401.

Ranero, C.R., Phipps Morgan, J., McIntosh, K., Reichert, C., 2003. Bending-related faulting and mantle serpentinization at the Middle America trench. Nature 425(6956), 367-373.

Reinecke, T., 1998. Prograde high- to ultrahigh-pressure metamorphism and exhumation of oceanic sediments at Lago di Cignana, Zermatt-Saas Zone, western Alps. Lithos 42(3-4), 147-189.

Rogers, G., Dragert, H., 2003. Episodic Tremor and Slip on the Cascadia Subduction Zone: The Chatter of Silent Slip. Science 300(5627), 1942-1943.

Rosenbaum, G., Lister, G.S., 2005. The Western Alps from the Jurassic to Oligocene: spatio-temporal constraints and evolutionary reconstructions. Earth-Science Reviews 69(3-4), 281-306.

Rowe, C.D., Moore, J.C., Meneghini, F., McKeirnan, A.W., 2005. Large-scale pseudotachylytes and fluidized cataclasites from an ancient subduction thrust fault. Geology 33(12), 937-940.

Rubatto, D., Hermann, J., 2001. Exhumation as fast as subduction? Geology 29(1), 3-6.

Rubatto, D., Hermann, J., 2003. Zircon formation during fluid circulation in eclogites (Monviso, Western Alps): implications for Zr and Hf budget in subduction zones. Geochimica et Cosmochimica Acta 67(12), 2173-2187.

Rutter, E.H., 1986. On the nomenclature of mode of failure transitions in rocks. Tectonophysics 122(3-4), 381-387.

Rutter, E.H., Brodie, K.H., 1995. Mechanistic interactions between deformation and metamorphism. Geological Journal 30(3-4), 227-240.

Rybacki, E., Dresen, G., 2000. Dislocation and diffusion creep of synthetic anorthite aggregates. Journal Geophysical Research 105(B11), 26017-26036.

Scambelluri, M., Muntener, O., Hermann, J., Piccardo, G.B., Trommsdorff, V., 1995. Subduction of water into the mantle: History of an Alpine peridotite. Geology 23(5), 459-462.

Schliestedt, M., 1990. Occurrences and stability conditions of low-temperature eclogites, Eclogite Facies Rocks, 1990 - Blackie.

Schrank, C.E., Handy, M.R., Fusseis, F., 2008. Multiscaling of shear zones and the evolution of the brittle-to-viscous transition in continental crust. Journal of Geophysical Research 113,(B01407).

Schwartz, S., Allemand, P., Guillot, S., 2001. Numerical model of the effect of serpentinites on the exhumation of eclogitic rocks: insights from the Monviso ophiolitic massif (Western Alps). Tectonophysics 342(1-2), 193-206.

Schwartz, S., Lardeaux, J.M., Guillot, S., Tricart, P., 2000. The diversity of eclogitic metamorphism in the Monviso ophiolitic complex, western Alps, Italy. Geodinamica Acta 13(2-3), 169-188.

Selverstone, J., Franz, G., Thomas, S., Getty, S., 1992. Fluid variability in 2 GPa eclogites as an indicator of fluid behavior during subduction. Contributions to Mineralogy and Petrology 112(2), 341-357.

Shea, W.T., Kronenberg, A.K., 1992. Rheology and Deformation Mechanisms of an Isotropic Mica Schist. Journal of Geophysical Research 97(B11), 15201-15237.

Sibson, R.H., 1986. Earthquakes and Rock Deformation in Crustal Fault Zones. Annual Review of Earth and Planetary Sciences 14(1), 149-175.

Spandler, C., Pettke, T., Rubatto, D., 2011. Internal and External Fluid Sources for Eclogite-facies Veins in the Monviso Meta-ophiolite, Western Alps: Implications for Fluid Flow in Subduction Zones. Journal of Petrology 52(6), 1207-1236.

Stern, R.J., 2004. Subduction initiation: spontaneous and induced. Earth and Planetary Science Letters 226(3-4), 275-292.

Stöckhert, B., 2002. Stress and deformation in subduction zones: insight from the record of exhumed metamorphic rocks. Geological Society, London, Special Publications 200(1), 255-274.

Strömgård, K.-E., 1973. Stress distribution during formation of boudinage and pressure shadows. Tectonophysics 16(3-4), 215-248.

Terry, M.P., Heidelbach, F., 2006. Deformation-enhanced metamorphic reactions and the rheology of high-pressure shear zones, Western Gneiss Region, Norway. Journal of Metamorphic Geology 24(1), 3-18.

Terry, R.D., Chilinger, G.V., 1955. Comparison charts for visual estimation of percentage composition. Journal of Sediment Petrology 25, 229–234.

Tilton, G.R., Schreyer, W., Schertl, H.P., 1991. Pb- Sr- Nd isotopic behavior of deeply subducted crustal rocks from the Dora Maira Massif, Western Alps, Italy-II: what is the age of the ultrahigh-pressure metamorphism? Contributions to Mineralogy and Petrology 108(1), 22-33.

Toyoshima, T., 1990. Pseudotachylite from the Main Zone of the Hidaka metamorphic belt, Hokkaido, northern Japan. Journal of Metamorphic Geology 8(5), 507-523.

Treagus, S.H., 1981. A theory of stress and strain variations in viscous layers, and its geological implications. Tectonophysics 72(1-2), 75-103.

Tricart, P., Schwartz, S., Sue, C., Lardeaux, J.-M., 2004. Evidence of synextension tilting and doming during final exhumation from analysis of multistage faults (Queyras Schistes lustrés, Western Alps). Journal of Structural Geology 26(9), 1633-1645.

Tullis, J., Yund, R.A., 1987. Transition from cataclastic flow to dislocation creep of feldspar: Mechanisms and microstructures. Geology 15(7), 606-609.

Ulmer, P., Trommsdorff, V., 1995. Serpentine Stability to Mantle Depths and Subduction-Related Magmatism. Science 268(5212), 858-861.

Watson, B., Brenan, J., 1987. Fluids in the lithosphere, 1. Experimentally-determined wetting characteristics of CO2H2O fluids and their implications for fluid transport, host-rock physical properties, and fluid inclusion formation. Earth and Planetary Science Letters 85(4), 497-515.

White, S.H., Burrows, S.E., Carreras, J., Shaw, N.D., Humphreys, F.J., 1980. On mylonites in ductile shear zones. Journal of Structural Geology 2(1-2), 175-187.

White, S.H., Knipe, R.J., 1978. Transformation- and reaction-enhanced ductility in rocks. Journal of the Geological Society 135(5), 513-516.

Whitney, D.L., Evans, B.W., 2010. Abbreviations for names of rock-forming minerals. American Mineralogist 95(1), 185-187.

Yamato, P., Agard, P., Burov, E., Le Pourhiet, L., Jolivet, L., Tiberi, C., 2007. Burial and exhumation in a subduction wedge: Mutual constraints from thermomechanical modeling and natural P-T-t data (Schistes Lustres, western Alps). Journal of Geophysical Research-Solid Earth 112(B7).

Zhang, J., Green, H.W., 2007. Experimental Investigation of Eclogite Rheology and Its Fabrics at High Temperature and Pressure. Journal of Metamorphic Geology 25(2), 97-115.

Zhang, J., Green, H.W., Bozhilov, K.N., 2006. Rheology of omphacite at high temperature and pressure and significance of its lattice preferred orientations. Earth and Planetary Science Letters 246(3-4), 432-443.

Zhao, D., Mishra, O.P., Sanda, R., 2002. Influence of fluids and magma on earthquakes: seismological evidence. Physics of The Earth and Planetary Interiors 132(4), 249-267.

Figure captions

Figure 1: Sketch showing a typical subduction zone and some of the key processes occurring along the plate interface. Mechanical coupling is maximum along the seismogenic zone (between 10-35km) where the plate boundary is possibly sealed (Audet et al., 2009). Episodic tremor and slip events (ETS) generally occur at the base of the seismogenic zone. Decoupling is believed to occur below due to fluid transfer across the plate interface and serpentinization of the overlying mantle wedge. Note that the oceanic mantle is also believed to be partially serpentinized before entering the trench.

Figure 2: **a**. Geological map of the working area showing the location of the main shear zones, the position of the units and the location of samples mentioned in text (modified after Lombardo et al., 1978 and Angiboust et al., 2011). The inset localizes the Monviso ophiolite within the Western Alps. **b**. Section across the Monviso ophiolite showing the disposition of the main tectonic units and tectonic relationships between them (dotted transect on Fig. 2a).

Figure 3: **a**. Field view of the Lago Superiore Unit showing the various lithologies and the location of the three main shear zones (USZ, ISZ, LSZ: upper, intermediate and lower shear zones, respectively) together with samples mentioned in the text. Deep shear zones (in red) are marked as thrusts on the picture. The USZ, reactivated as a major detachment zone during late exhumation processes, is lined by dark black rectangles. **b**. Field view of a rounded block of Fe-Ti metagabbro embedded within LSZ serpentinites (Punta Forcione: N 44° 40’ 38.1”; E 07° 07’

39.8”). **c.** Drawing illustrating a disaggregated block and associated disseminated fragments within a serpentinite/talcschist matrix (Punta Murel: N 44° 39’ 00.5”; E 07° 07’ 55.4”). **d.** A strongly foliated mylonite where omphacite (Omp) and garnet (Grt) have been clearly segregated in two distinct domains (hammer for scale). Note that whitish pseudomorphs after lawsonite (Ps. Lws) are concentrated in omphacite domains. **e**. Picture of typical eclogite breccias found at the surface of blocks embedded within the Lower Shear Zone (LSZ), showing variably sized and oriented fragments of eclogite facies mylonites cemented by omphacite. **f.** Drawing of the foliation trend within an eclogite-facies breccia from Colle di Luca (Fig. 2a) emphasizing the rotation of the fragments at the block surface.

Figure 4: a. Contact between a mylonitized eclogite fragment and a vein filled by omphacite and pseudomorphs after lawsonite at the surface of a brecciated eclogitic block from the LSZ (N 44° 39’ 52.8”; E 07° 07’ 50.3”). **b.** Lawsonite eclogite sample occurring in a low-strained domain at the block surface showing remarkably large lawsonite pseudomorphs (up to 1cm in length) in a weakly deformed matrix (Punta Murel; Fig.2a). **c.** A mylonitic foliation consisting of garnet, omphacite and rutile (right) crosscut by a vein (left) filled by lawsonite and omphacite (lawsonite is now pseudomorphed by epidote and paragonite). **d.** Boudinaged mylonitic fragment wrapped within a later foliation consisting of omphacite, garnet and lawsonite (LSZ). Mineral abbreviations as in figure 3.

Figure 5: a. Scanned thin section of a moderately strained eclogite from a block embedded within serpentinite from USZ (Fig. 2a), showing relatively well preserved relicts of omphacite porphyroclasts (after augite) embedded within an omphacite-rich foliated domain. **b.** Quantified chemical map of a garnet crystal magnesium content (wt.%) of sample USZ-69, showing a typical zoning pattern (enrichment in Mg towards the rims) and the absence of healed fractures. **c.** Back-scattered Electron (BSE) view of an Fe-Ti metagabbro mylonite from Lago Superiore Area

showing pseudomorphs after lawsonite growing along the omphacitic foliation. Dismembered rutile ribbons underline the foliation. **d**. BSE picture of a garnet showing two distinct garnet generations with a clear Ca-rich core and a dark Mg-rich rim. A dark complex network of healed Mg-rich fractures connected on the garnet rim crosscuts the garnet core. Garnet chemical composition across the fracture (transect a-b) is given in Supplementary material 3. **e.** Chemical map of Mg content (counts) of the mylonitic matrix from sample ISZ-17. **f.** Chemical map of Mg content (wt.%) of a garnet from sample ISZ-49 exhibiting a very complex pattern of Mg-enriched healed fractures. **g**. Scanned thin section of a mylonitic sample showing the mylonitic foliation deflected around an omphacite-filled crack-seal vein. **h**. Scanned thin section of sample LSZ-42 (courtesy of D. Waters) showing numerous phengite and pseudomorphed lawsonite crystals along the eclogitic foliation. Abbreviations after Whitney and Evans (2010).

Figure 6: a. Chemical maps of a garnet from a chlorite-eclogite sample from the LSZ (LSZ-23). **b.** Sketches depicting the successive steps of garnet growth. A first garnet (Garnet I) generation is fractured and healed by a Mn-Ca rich garnet composition (white dotted line square). A second fracturing episode is attested by the presence of a very complex fracture pattern cemented by a Mg-rich composition (Garnet II). **c.** Core to rim zoning profiles of the garnet composition. **d.** These successive events can be interpreted in terms of cyclic variation of relative shear stress associated with movement along the shear zone. See discussion for details.

Figure 7: a. Plot of the bulk rock composition in the ACF triangle (with F=FeO) for the mylonites sampled in the Intermediate (ISZ) and Lower (LSZ) Shear Zones distinguishing the different types of mylonites identified on petrographic observation and the trend in FeO depletion associated with water-saturated mylonitization (growth of lawsonite). **b.** Smoothed, normalized garnet core-rim transects for eleven samples from the three different shear zones. Iron depletion is

systematically observed at the rim of garnet from LSZ while it is absent within garnet from unaltered or ISZ samples. The red arrow localizes the relative position of incipient depletion.

Figure 8: a. Relative chronology of events (and associated P-T position) observed on eclogite Fe-Ti metagabbro mylonites boudins along the ISZ and LSZ. Igneous texture (step 1) is progressively blurred by mylonitization processes (step 2) leading to grain size reduction, garnet fracturing and phase segregation. Variable amounts of hydrous phases crystallized depending on the amount of water available during mylonitization. Eclogite facies breccias (step 3), commonly found along the LSZ are generally cemented by omphacite +/- lawsonite +/- garnet. These brecciated fragments (Fig. 3f) may be embedded as boudins in a later lawsonite eclogite-facies foliation (step 4). The P-T diagram at the background shows the P-T path for the LSU ophiolite, the location of the main metamorphic facies and the relative position of the four steps identified. Note that the presence of lawsonite (now pseudomorphed by epidote), omphacite and garnet in all textural positions constrains these events to the lawsonite-eclogite facies. **b.** Schematic drawing at the scale of the Lago Superiore unit, showing the location of the different shear zones and the location of the four steps mentioned above. Our results indicate that substantial fluid flow occurred along the LSZ, whereas only short range localized fluid flow within the ISZ.

Figure 9: a. Plot of differential strength (thick line) and viscosities (dotted line) against the same cross-section using the following flow laws: calcschists (micaschist: Shea and Kronenberg, 1992), basalts (omphacitite: Zhang et al., 2006), gabbros Fe-Ti (eclogite: Jin et al., 2001), gabbros Mg-Al (diabase: Mackwell et al., 1995), serpentinite (serpentinite: Hilairet et al., 2007) at 550°C and with a strain rate of 10^{-14}. More details on the construction of the profile are given in Appendix C. **b.** Finite strain envelope across the described section, inferred from field observations and strain markers, showing that strain is strongly localized along the shear zones. **c.** Section across the Lago Superiore Unit showing the lithologies and the location of the three main shear zones. Arrows

along the shear zones represent normal movement during late exhumation processes (Philippot and Van Roermund, 1992).

Figure 10: a. Sketch representing the Lago Superiore ophiolite slice at the onset of mylonitization. Deformation is first localized on the ISZ, at the boundary between basalts and gabbros (red dotted line). **b.** Ongoing shearing along the plate interface is responsible for dismembering and fragmentation of eclogite blocks detached from the ISZ. **c.** The whole Lago Superiore unit finally detaches from the downgoing slab and the bulk of the deformation is now localized at the base of the serpentinite sole. Monviso unit, which detaches from the slab at c. 65-70km is not represented here. **d.** P-T paths from Angiboust et al. (2011) for both Monviso and Lago Superiore Units. **e**. Eclogite facies shear zone activity is restricted to the vicinity of peak conditions (i.e. 550°C, 26 kbar). Juxtaposition with the adjacent Monviso Unit occurs in the epidote blueschist facies during exhumation in the subduction channel (Schwartz et al., 2000). The relative timing of shear zone activity is based on the intensity of metamorphism recorded by the rocks from the different shear zones.

Table 1: Summary of field, structural and petrological observations with emphasis on the lenses and/or blocks dispersed within the three main shear zones. Thermobarometric results are from Angiboust et al. (2011).

Table 2: Synthesis of peak paragenesis and relative phase abundances in the selected set of samples from the three shear zones described in the text.

Supplementary material 1: Detailed geological maps of selected areas along the ISZ and LSZ. Position of these close-up views is shown in Figure 2.

Supplementary material 2: Chemical map comparing garnet zoning pattern from USZ and ISZ. A "classical" (i.e. a smooth decrease in Ca-Mn garnet content from core to rim) undisturbed zoning pattern is observed for the sample embedded within the USZ serpentinites (USZ-69). Garnet from a mylonite from ISZ exhibits two distinct generations: the core of Grt I is enriched in Mn-Ca while the rim (Grt II) is enriched in Mg-Fe. An intense fracture network, characterized by healing with Mg-enriched Grt composition, crosscuts Grt I.

Supplementary material 3: Garnet end-member molar fraction from EMP chemical analyses for the transect a-b (Fig. 5d) across a healed fracture showing a clear enrichment in Mg along the fracture.

Supplementary material 4: Summary of bulk-rock estimates performed for this study and average composition obtained for each rock type. GPS coordinates of each sample are also given.

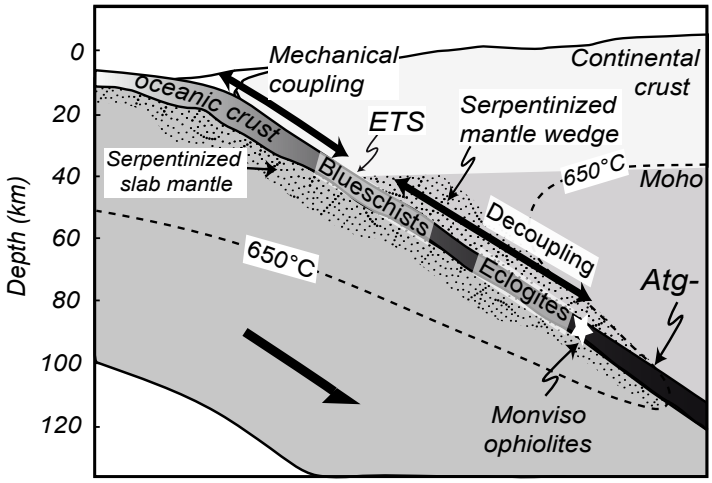
0
20
40
60
80
100
120
Depth (km)
Mechanical coupling
Continental crust
oceanic crust
ETS
Serpentinized mantle wedge
Serpentinized slab mantle
Blueschists
650°C
Moho
Decoupling
650°C
Eclogites
Atg-
Monviso ophiolites

Figure 1

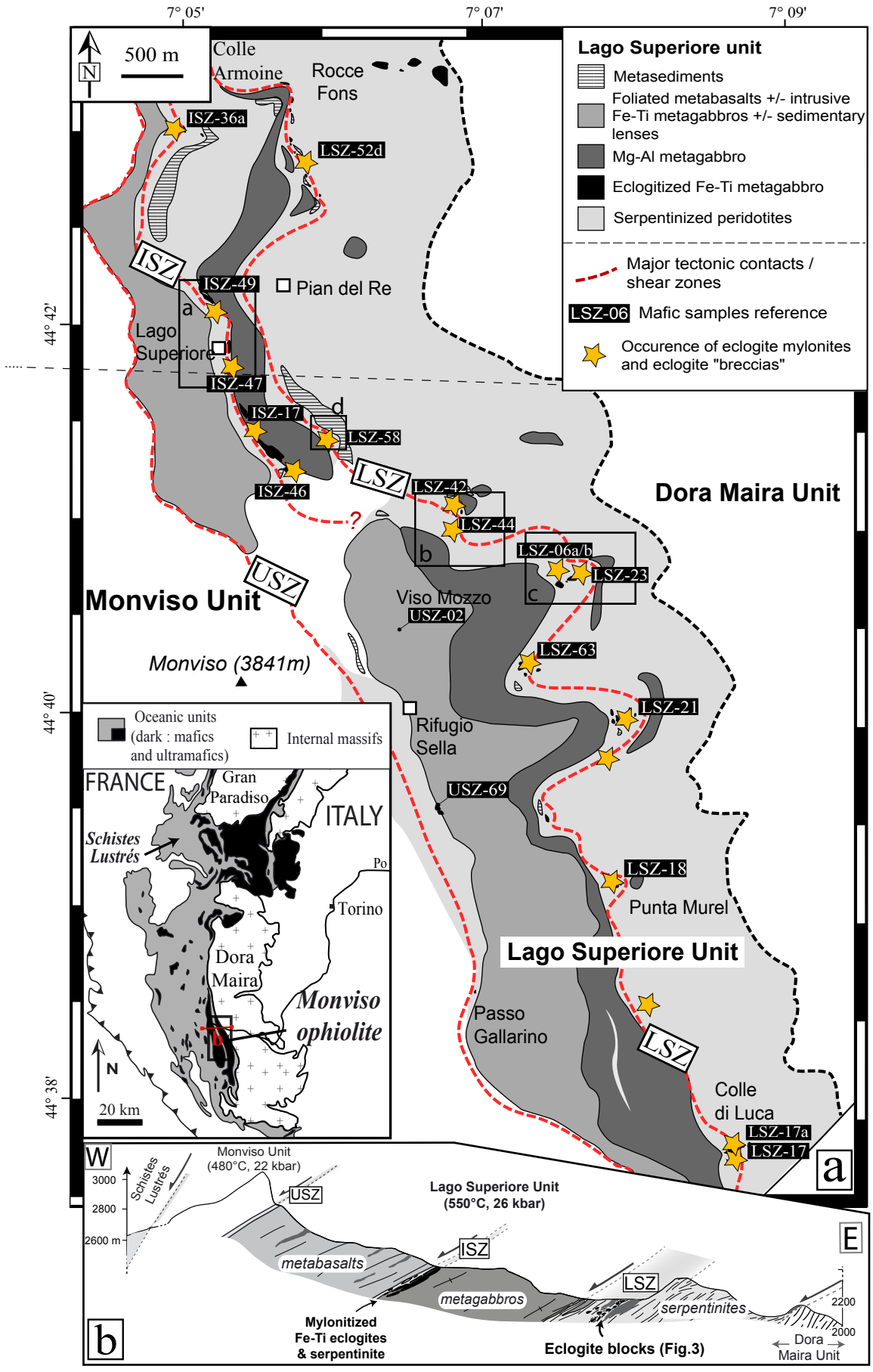
7° 05'
7° 07'
7° 09'
44° 42'
44° 40'
44° 38'
500 m
N
Colle Armoine
Rocce Fons
ISZ-36a
LSZ-52d
ISZ
ISZ-49
Pian del Re
a
Lago Superiore
ISZ-47
ISZ-17
d
LSZ-58
ISZ-46
LSZ
LSZ-42
LSZ-44
b
LSZ-06a/b
LSZ-23
c
USZ
Monviso Unit
Viso Mozzo
USZ-02
Monviso (3841m)
LSZ-63
LSZ-21
Rifugio Sella
USZ-69
LSZ-18
Punta Murel
Lago Superiore Unit
Passo Gallarino
LSZ
Colle di Luca
LSZ-17a
LSZ-17
a
Dora Maira Unit
Lago Superiore unit
Metasediments
Foliated metabasalts +/- intrusive Fe-Ti metagabbros +/- sedimentary lenses
Mg-Al metagabbro
Eclogitized Fe-Ti metagabbro
Serpentinized peridotites
Major tectonic contacts / shear zones
LSZ-06 Mafic samples reference
Occurence of eclogite mylonites and eclogite "breccias"
Oceanic units (dark : mafics and ultramafics)
Internal massifs
FRANCE
ITALY
Gran Paradiso
Schistes Lustrés
Po
Torino
Dora Maira
Monviso ophiolite
N
20 km
W
E
3000
2800
2600 m
Schistes Lustrés
Monviso Unit (480°C, 22 kbar)
USZ
Lago Superiore Unit (550°C, 26 kbar)
ISZ
metabasalts
metagabbros
LSZ
serpentinites
2200
2000
Dora Maira Unit
Mylonitized Fe-Ti eclogites & serpentinite
Eclogite blocks (Fig.3)
b

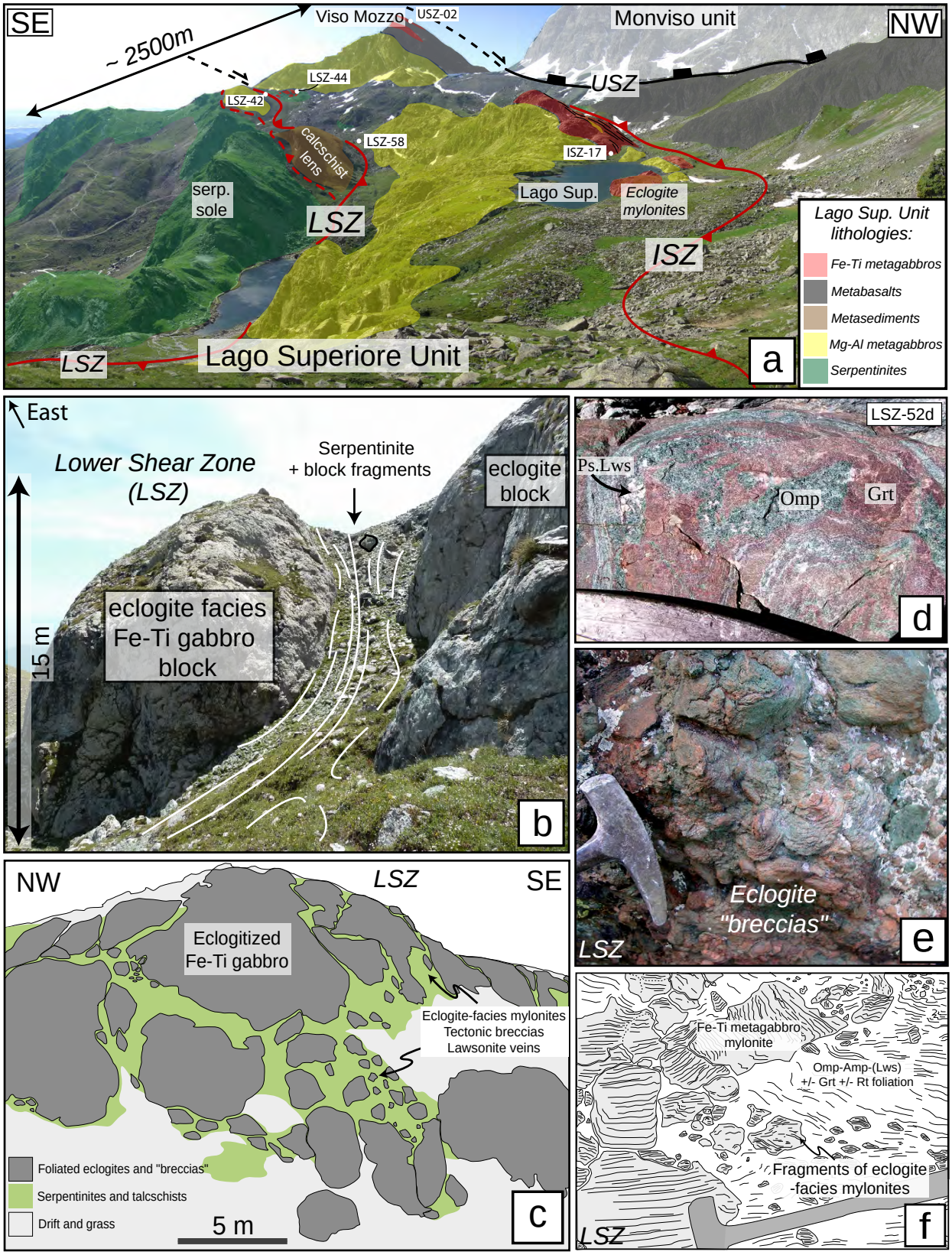
SE
NW
~ 2500m
Viso Mozzo
USZ-02
Monviso unit
LSZ-44
LSZ-42
USZ
calcschist lens
LSZ-58
ISZ-17
serp. sole
LSZ
Lago Sup.
Eclogite mylonites
ISZ
Lago Sup. Unit lithologies:
Fe-Ti metagabbros
Metabasalts
Metasediments
Mg-Al metagabbros
Serpentinites
LSZ
Lago Superiore Unit
a
East
Lower Shear Zone (LSZ)
Serpentinite + block fragments
eclogite block
eclogite facies Fe-Ti gabbro block
15 m
b
LSZ-52d
Ps.Lws
Omp
Grt
d
Eclogite "breccias"
LSZ
e
NW
LSZ
SE
Eclogitized Fe-Ti gabbro
Eclogite-facies mylonites
Tectonic breccias
Lawsonite veins
Foliated eclogites and "breccias"
Serpentinites and talcschists
Drift and grass
5 m
c
Fe-Ti metagabbro mylonite
Omp-Amp-(Lws) +/- Grt +/- Rt foliation
Fragments of eclogite -facies mylonites
LSZ
f

Figure 3

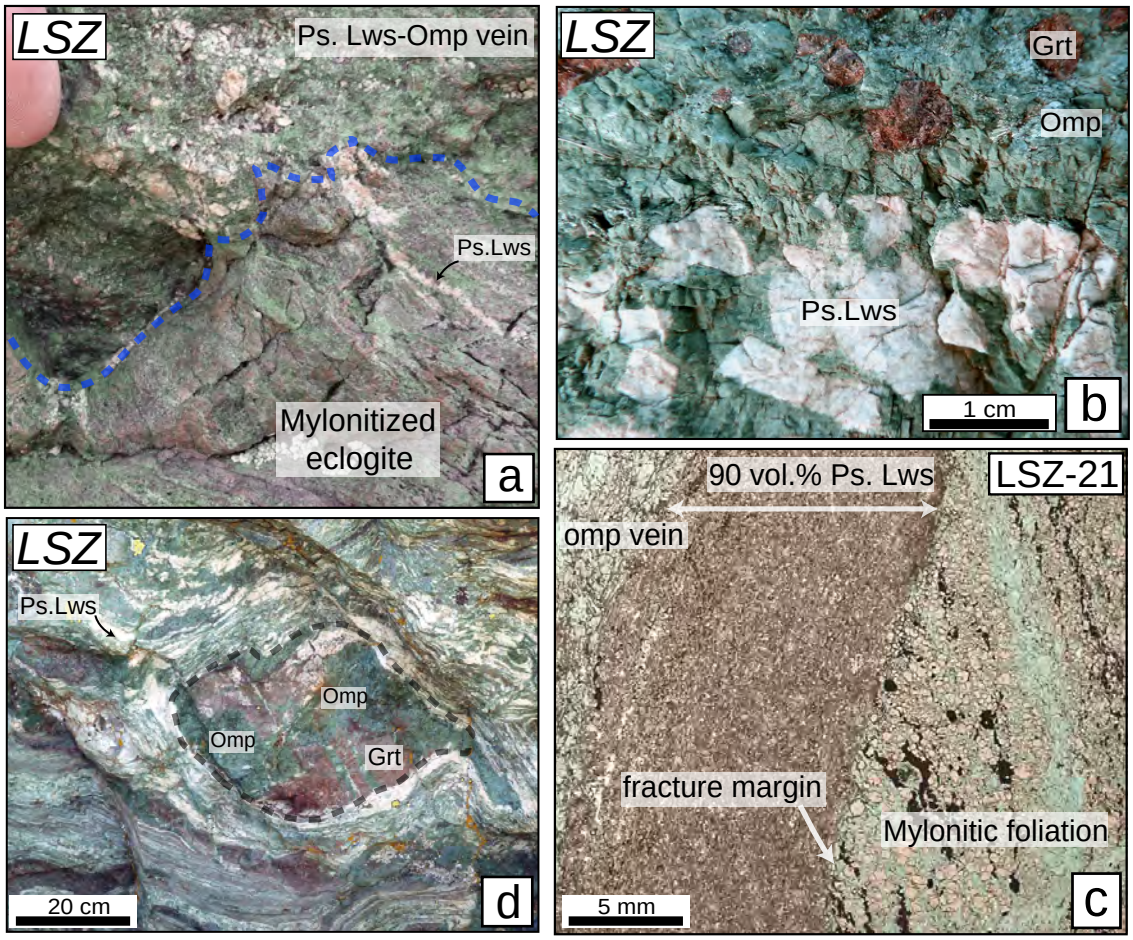
LSZ
Ps. Lws-Omp vein
Ps.Lws
Mylonitized
eclogite
a
LSZ
Grt
Omp
Ps.Lws
1 cm
b
LSZ
Ps.Lws
Omp
Omp
Grt
20 cm
d
90 vol.% Ps. Lws
LSZ-21
omp vein
fracture margin
Mylonitic foliation
5 mm
c

Figure 4

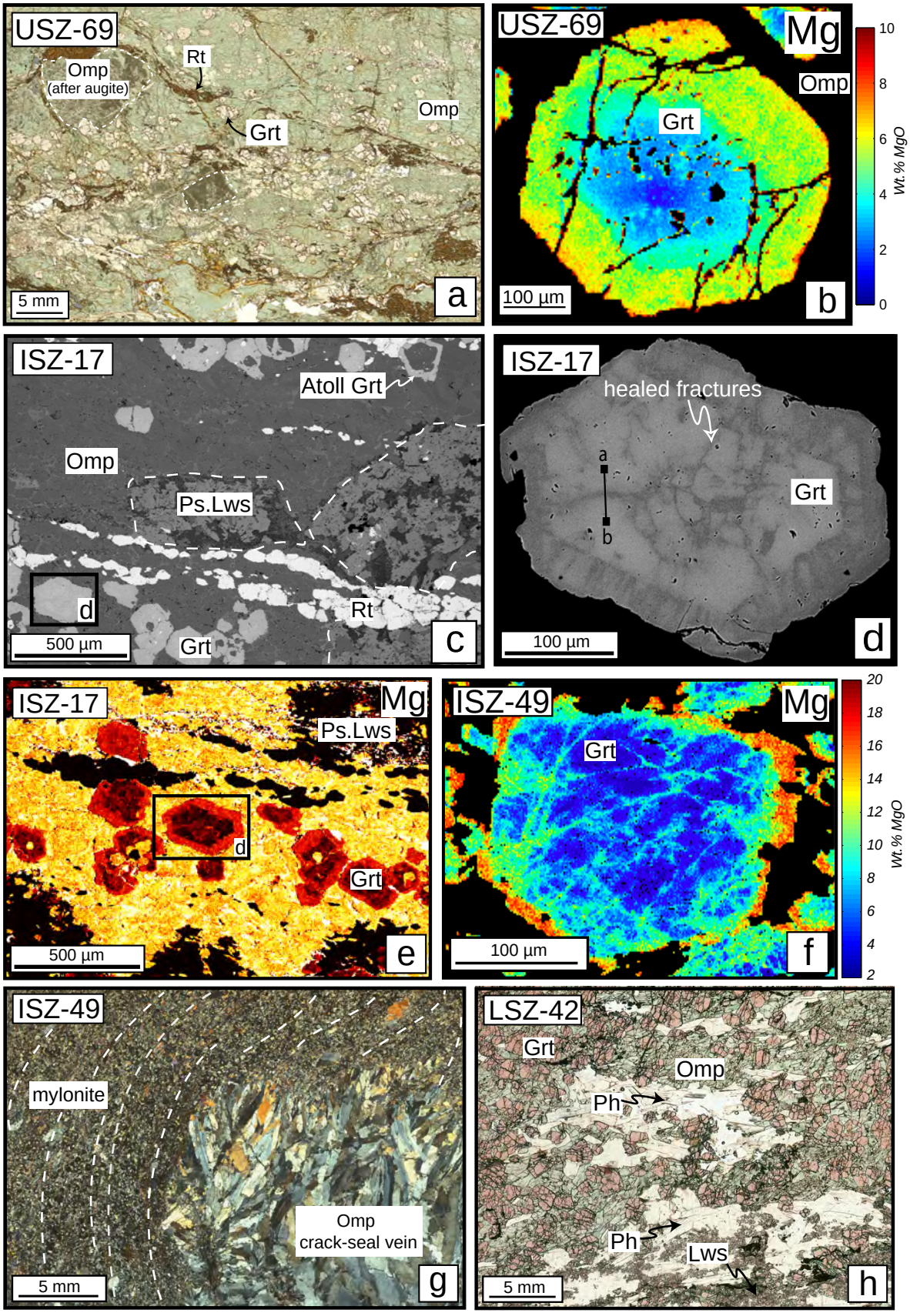
USZ-69
Omp
(after augite)
Rt
Grt
Omp
5 mm
a
USZ-69
Mg
Omp
Grt
100 µm
b
10
8
6
4
2
0
Wt.% MgO
ISZ-17
Atoll Grt
Omp
Ps.Lws
d
Rt
500 µm
Grt
c
ISZ-17
healed fractures
a
b
Grt
100 µm
d
ISZ-17
Mg
Ps.Lws
d
Grt
500 µm
e
ISZ-49
Mg
Grt
100 µm
f
20
18
16
14
12
10
8
6
4
2
Wt.% MgO
ISZ-49
mylonite
Omp
crack-seal vein
5 mm
g
LSZ-42
Grt
Omp
Ph
Ph
Lws
5 mm
h

Figure 5

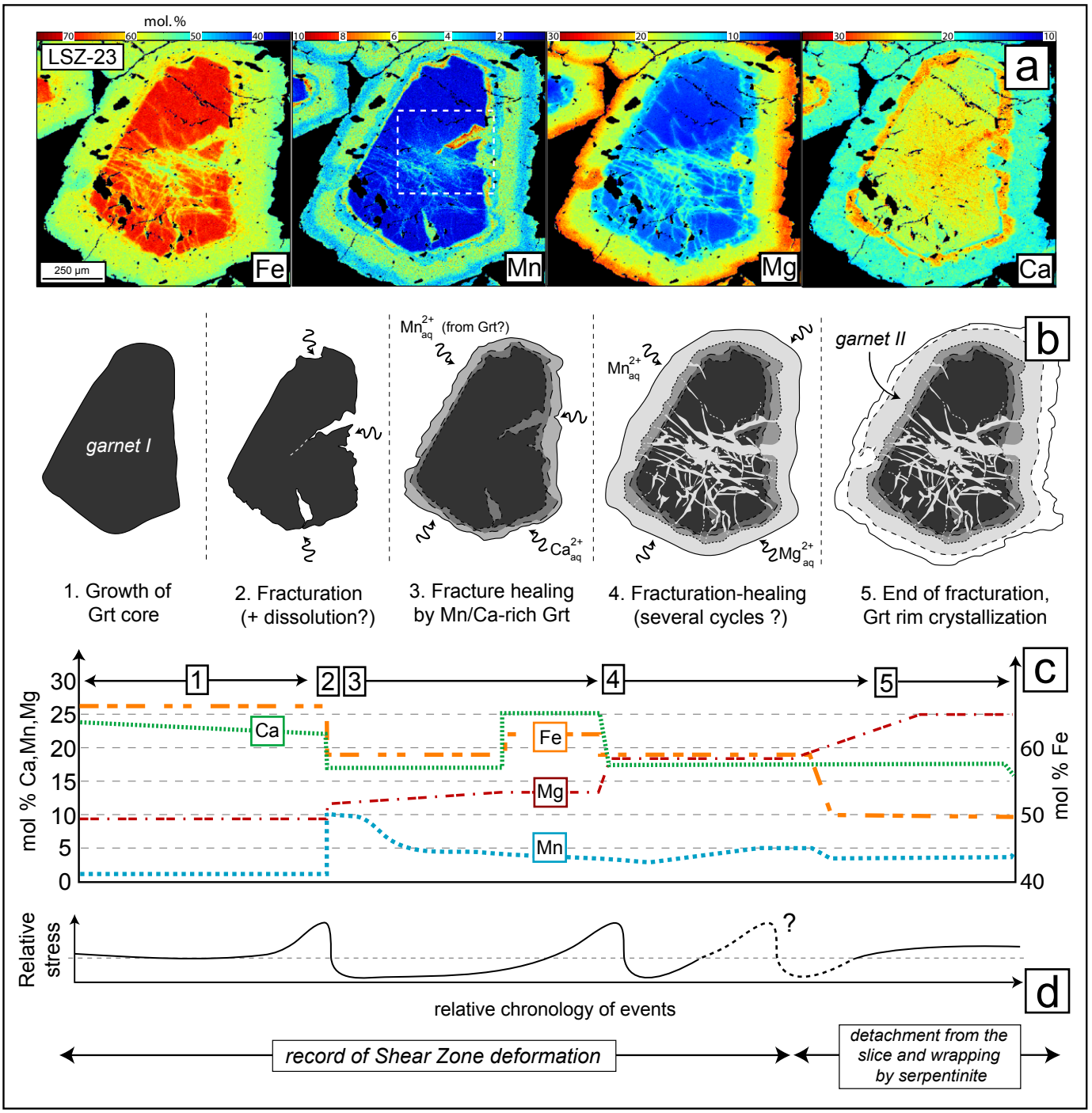
mol.%
LSZ-23
a
Fe
Mn
Mg
Ca
250 µm
garnet I
Mn^{2+}_{aq} (from Grt?)
Ca^{2+}_{aq}
Mn^{2+}_{aq}
Mg^{2+}_{aq}
garnet II
b
1. Growth of Grt core
2. Fracturation (+ dissolution?)
3. Fracture healing by Mn/Ca-rich Grt
4. Fracturation-healing (several cycles ?)
5. End of fracturation, Grt rim crystallization
c
mol % Ca,Mn,Mg
mol % Fe
Ca
Fe
Mg
Mn
Relative stress
?
d
relative chronology of events
record of Shear Zone deformation
detachment from the slice and wrapping by serpentinite

Figure 6

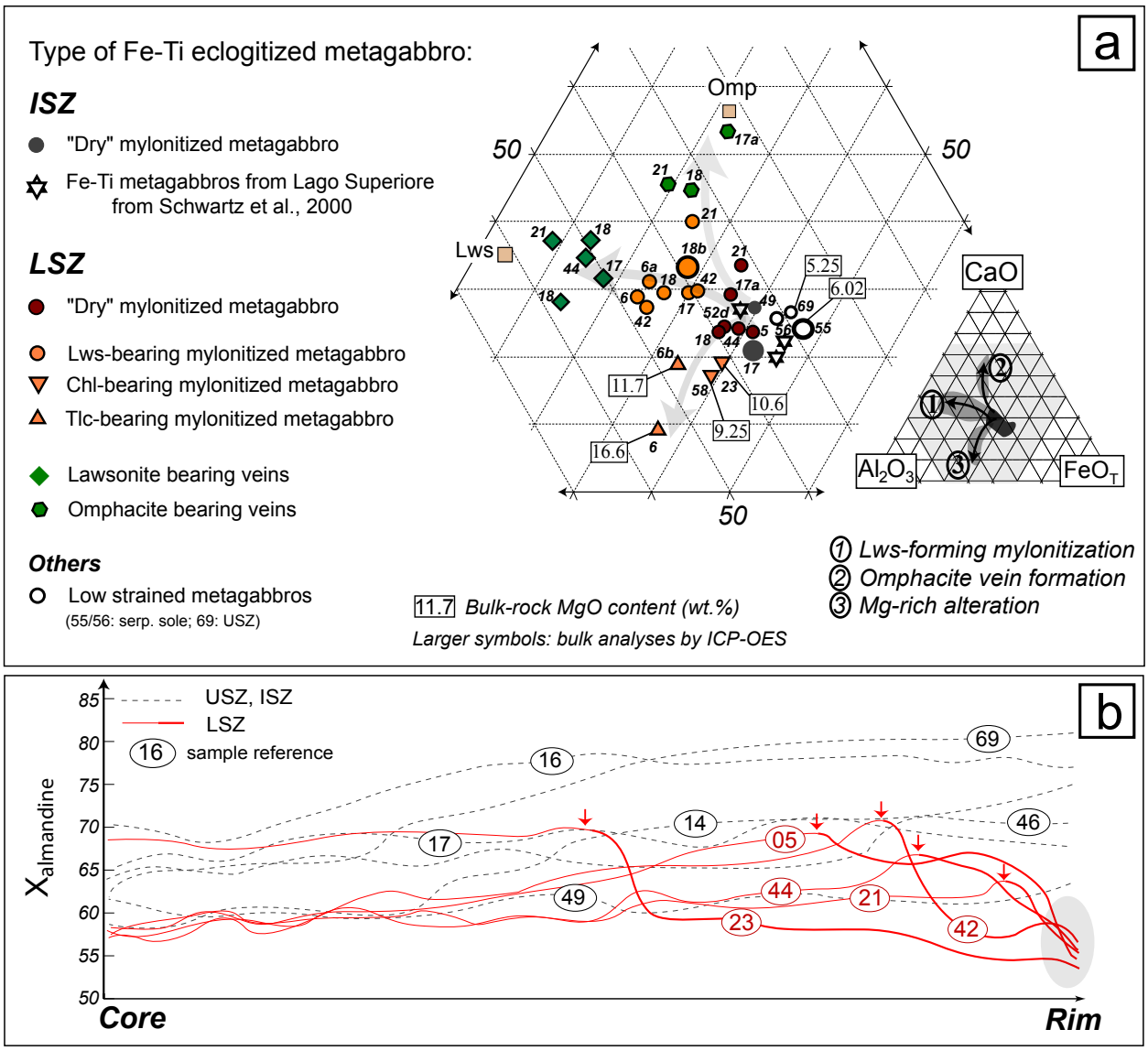
a
Type of Fe-Ti eclogitized metagabbro:
ISZ
"Dry" mylonitized metagabbro
Fe-Ti metagabbros from Lago Superiore from Schwartz et al., 2000
LSZ
"Dry" mylonitized metagabbro
Lws-bearing mylonitized metagabbro
Chl-bearing mylonitized metagabbro
Tlc-bearing mylonitized metagabbro
Lawsonite bearing veins
Omphacite bearing veins
Others
Low strained metagabbros
(55/56: serp. sole; 69: USZ)
Omp
Lws
50
50
50
5.25
6.02
11.7
10.6
9.25
16.6
CaO
Al2O3
FeOT
1 Lws-forming mylonitization
2 Omphacite vein formation
3 Mg-rich alteration
11.7 Bulk-rock MgO content (wt.%)
Larger symbols: bulk analyses by ICP-OES
b
USZ, ISZ
LSZ
16 sample reference
Xalmandine
85
80
75
70
65
60
55
50
Core
Rim

Figure 7

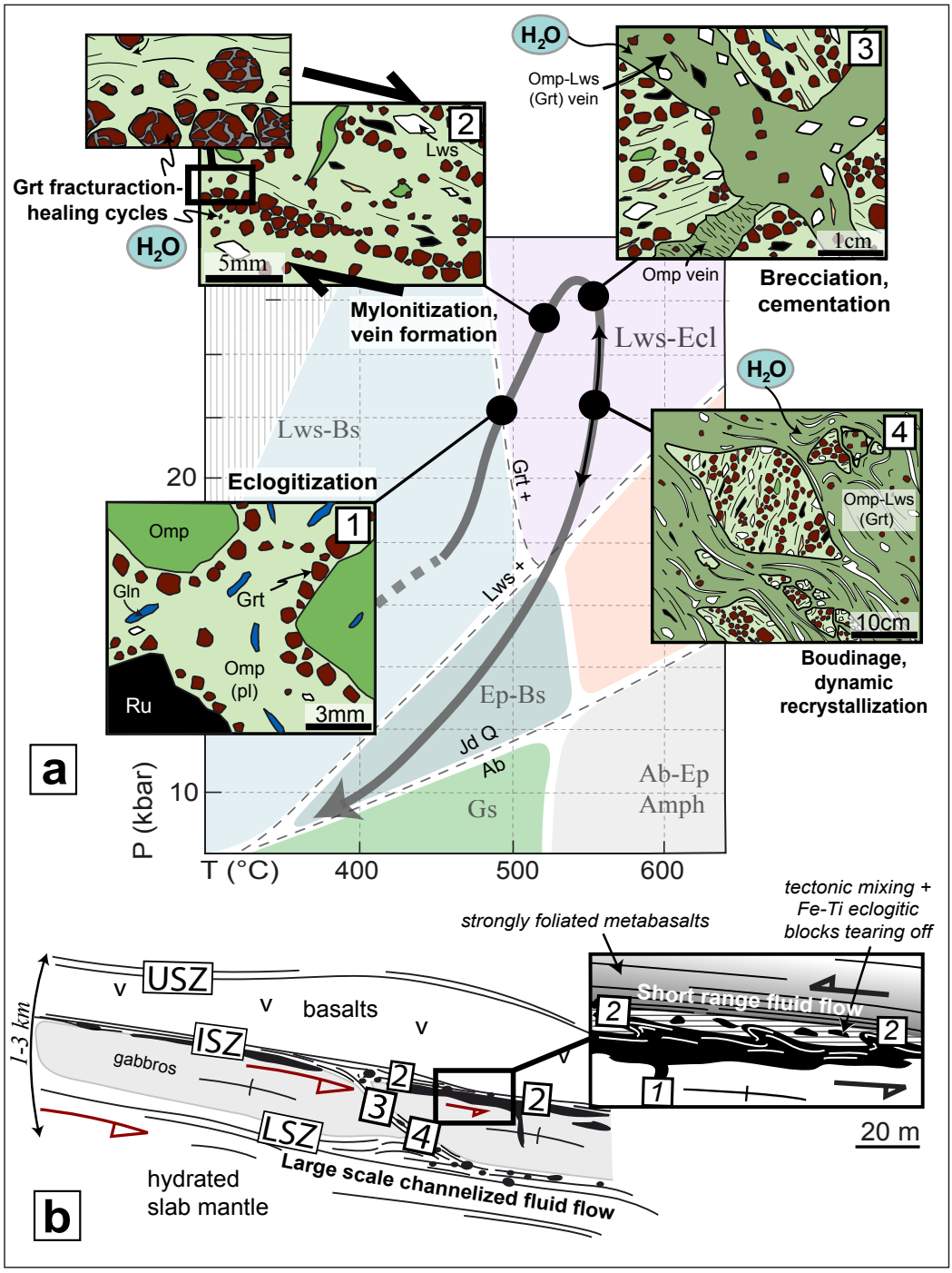
H2O
Omp-Lws
(Grt) vein
3
1cm
Omp vein
Brecciation,
cementation
2
Lws
Grt fracturaction-
healing cycles
H2O
5mm
Mylonitization,
vein formation
Lws-Ecl
H2O
Lws-Bs
4
Omp-Lws
(Grt)
10cm
Boudinage,
dynamic
recrystallization
20
Eclogitization
Omp
1
Gln
Grt
Omp
(pl)
Ru
3mm
Grt +
Lws + L
Ep-Bs
Jd Q
Ab
Gs
Ab-Ep
Amph
a
P (kbar)
10
T (°C)
400
500
600
tectonic mixing +
Fe-Ti eclogitic
blocks tearing off
strongly foliated metabasalts
Short range fluid flow
2
2
1
20 m
USZ
basalts
ISZ
gabbros
1-3 km
2
3
4
2
LSZ
Large scale channelized fluid flow
hydrated
slab mantle
b

Figure 8

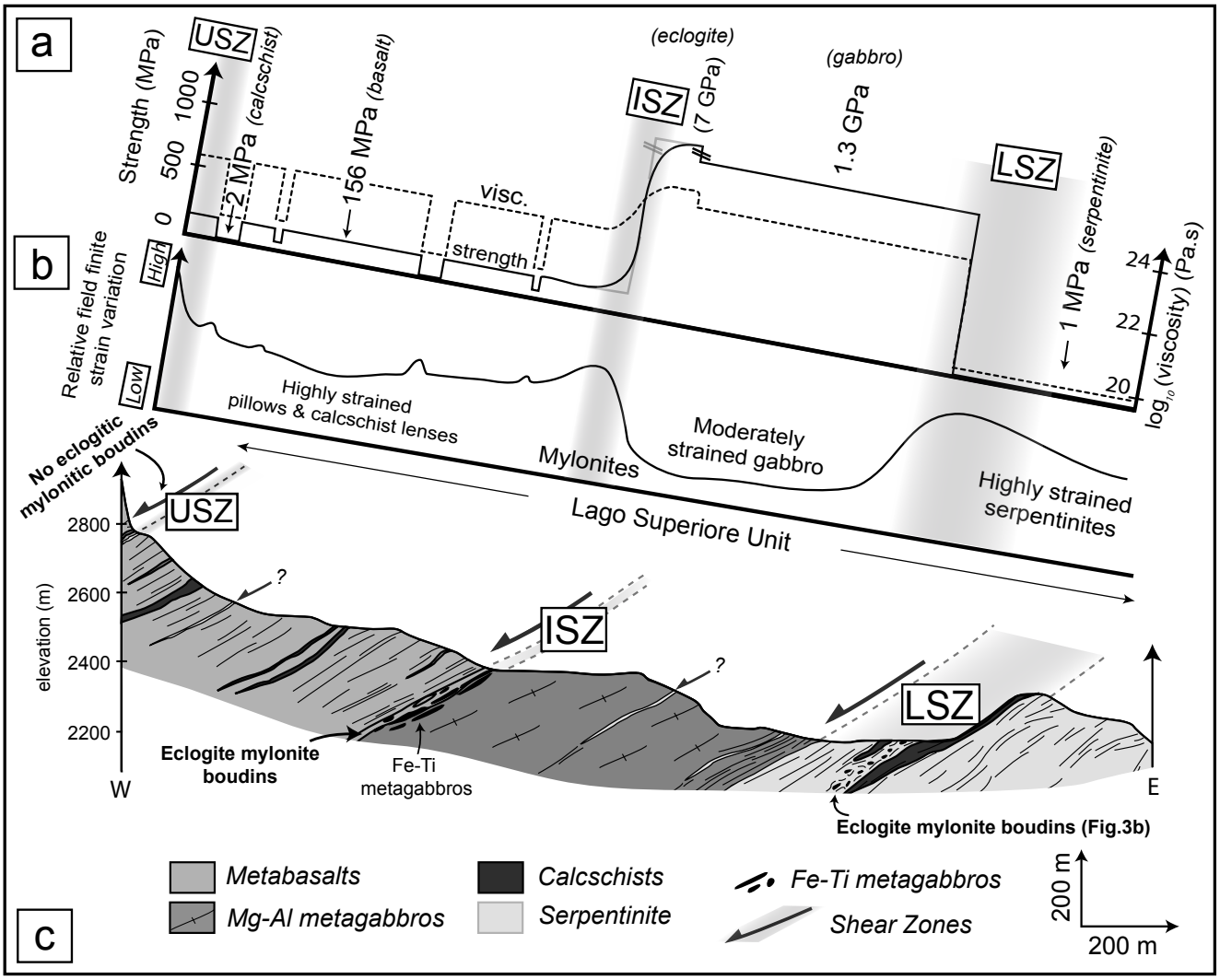
a
USZ
Strength (MPa)
1000
500
0
2 MPa (calcschist)
156 MPa (basalt)
visc.
strength
(eclogite)
ISZ
(7 GPa)
(gabbro)
1.3 GPa
LSZ
1 MPa (serpentinite)
24
22
20
log10 (viscosity) (Pa.s)
b
High
Low
Relative field finite strain variation
Highly strained pillows & calcschist lenses
Mylonites
Moderately strained gabbro
Highly strained serpentinites
Lago Superiore Unit
No eclogitic mylonitic boudins
USZ
2800
2600
2400
2200
elevation (m)
?
ISZ
?
LSZ
Eclogite mylonite boudins
Fe-Ti metagabbros
W
E
Eclogite mylonite boudins (Fig.3b)
c
Metabasalts
Mg-Al metagabbros
Calcschists
Serpentinite
Fe-Ti metagabbros
Shear Zones
200 m
200 m

Figure 9

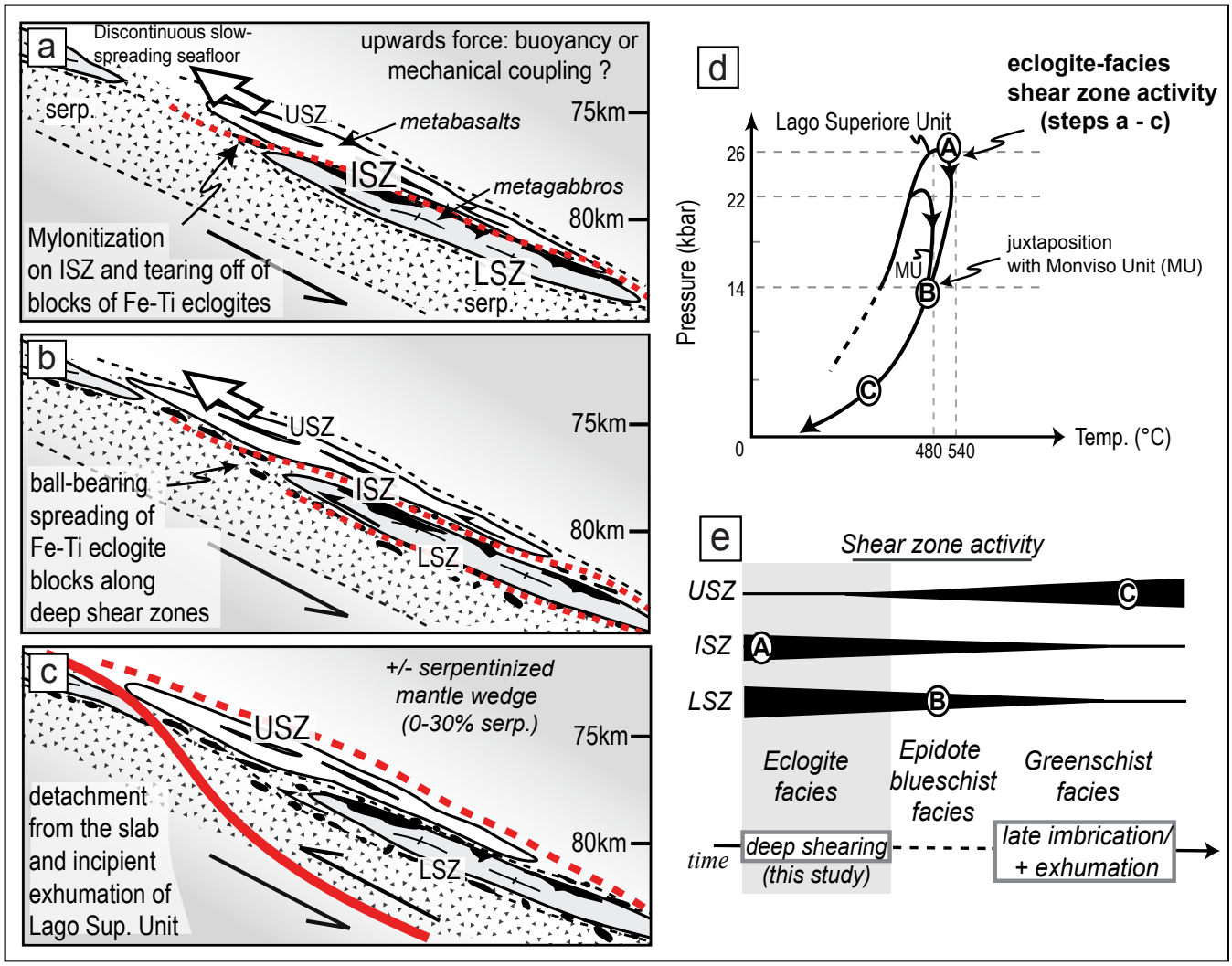
a
Discontinuous slow-spreading seafloor
upwards force: buoyancy or mechanical coupling ?
serp.
USZ
metabasalts
75km
ISZ
metagabbros
80km
Mylonitization on ISZ and tearing off of blocks of Fe-Ti eclogites
LSZ
serp.
b
USZ
75km
ball-bearing spreading of Fe-Ti eclogite blocks along deep shear zones
ISZ
80km
LSZ
c
+/- serpentinized mantle wedge (0-30% serp.)
USZ
75km
detachment from the slab and incipient exhumation of Lago Sup. Unit
80km
LSZ
d
eclogite-facies shear zone activity (steps a - c)
Lago Superiore Unit
A
26
22
Pressure (kbar)
juxtaposition with Monviso Unit (MU)
MU
B
14
C
0
480 540
Temp. (°C)
e
Shear zone activity
USZ
C
ISZ
A
LSZ
B
Eclogite facies
Epidote blueschist facies
Greenschist facies
time
deep shearing (this study)
late imbrication/ + exhumation

Figure 10